Quasi#periodic Oscillations from Rayleigh# Taylor and Kelvin#Helmholtz Instability at a Disk# Magnetosphere Interface

Quasi-Periodic Oscillations from Rayleigh-Taylor and Kelvin-Helmholtz Instability at a Disk-Magnetosphere Interface

Li-Xin Li[1] and Ramesh Narayan

Harvard-Smithsonian Center for Astrophysics, Cambridge, MA 02138, USA

lli,rnarayan@cfa.harvard.edu

ABSTRACT

We consider the interface between an accretion disk and a magnetosphere surrounding the accreting mass. We argue that such an interface can occur not only with a magnetized neutron star but also sometimes with an unmagnetized neutron star or a black hole. The gas at the magnetospheric interface is generally Rayleigh-Taylor unstable and may also be Kelvin-Helmholtz unstable. Because of these instabilities, modes with low azimuthal wavenumbers m are expected to grow to large amplitude. It is proposed that the resulting nonaxisymmetric structures contribute to the high frequency quasi-periodic oscillations that have been seen in neutron-star and black-hole X-ray binaries. The mode oscillation frequencies are calculated to be approximately equal to $m\Omega_m$, where Ω_m is the angular velocity of the accreting gas at the magnetospheric radius. Thus, mode frequencies should often be in the approximate ratio 1:2:3, etc. If the pressure of the gas in the disk is not large, then the $m = 1$ mode will be stable. In this case, the mode frequencies should be in the approximate ratio 2:3, etc. There is some observational evidence for such simple frequency ratios.

Subject headings: accretion, accretion disks — black hole physics — magnetic fields — MHD — instabilities — stars: oscillations — X-rays: binaries — X-rays: stars

1. Introduction

The study of the timing properties of X-ray binaries and, in particular, quasi-periodic oscillations (QPOs) in these sources, has for long been a major area of research (see van der

[1]Chandra Fellow

Klis 2000 and Remillard et al. 2002b for recent reviews, and Lewin, van Paradijs, & van der Klis 1988 for a discussion of earlier observations). The field has become especially active in recent years after the launch of the *Rossi X-Ray Timing Explorer* (*RXTE*; Bradt, Rothschild, & Swank 1993) with its superb timing capability. Among the divergent phenomenology of QPOs observed in X-ray binaries, of particular interest are the "kilohertz QPOs," which have frequencies $\sim 10^2 - 10^3$Hz.

About twenty accreting neutron-star sources and five accreting black-hole sources are known to exhibit kHz QPOs (van der Klis 2000; Remillard et al. 2002b). These QPOs often appear in pairs (so called "twin QPOs"), with the frequency difference being anticorrelated to the QPO frequencies (van der Klis 2000; Di Salvo, Méndez, & van der Klis 2003, see, however, Migliari, van der Klis, & Fender 2003). In many neutron star systems the frequency difference appears to be related to the spin frequency of the neutron star (van der Klis 2000; Wijnands et al. 2003). At the same time, in several sources, the twin kHz QPO frequencies seem to occur in the ratio of simple integers, with a frequency ratio of 2:3 being common in both black hole and neutron star systems (Abramowicz & Kluzniak 2001; Abramowicz et al. 2003; Remillard et al. 2002a).

Kilohertz QPOs occur at a similar frequency in neutron star sources that differ in X-ray luminosity by more than two orders of magnitude. Moreover, the QPO frequency in a given source seems to track the fluctuation in the X-ray intensity from average for that source rather than the absolute luminosity of the source (van der Klis 1997, 1998, 2000; Zhang, Strohmayer, & Swank 1997). Furthermore, there is a surprising continuity of QPO properties between black hole and neutron star binaries (Psaltis, Belloni & van der Klis 1999; Belloni, Psaltis & van der Klis 2002). The continuity even appears to extend to white dwarfs (Warner, Woudt & Pretorius 2003).

Because of their high frequencies, kHz QPOs must be produced by processes close to the accreting mass. However, since these QPOs have been observed in both neutron-star and black-hole X-ray binaries, the oscillations are unlikely to be associated with the surface of the accreting object. Instead, it seems likely that the kilohertz QPOs originate in the accretion flow surrounding the central mass. Motivated by this argument, a variety of accretion-based models have been proposed to explain the oscillations (Lewin, van Paradijs, & van der Klis 1988; van der Klis 2000, and references therein).

The classical beat frequency model for QPOs in neutron-star sources proposes that one of the kHz QPOs is associated with the Keplerian frequency of the orbiting gas at the inner edge of the accretion disk and that the second kHz QPO represents a beat phenomenon between the orbiting gas and the spin of the central star (Alpar & Shaham 1985; Lamb et al. 1985; Strohmayer et al. 1996; Miller, Lamb, & Psaltis 1998; Lamb & Miller 2001). This model

predicts that the frequency difference between the two kHz QPOs should be equal to the spin frequency of the neutron star and should be constant. However, observations show that the separation is not a constant: it generally decreases when the QPO frequencies increase. The frequency difference is also observed not to be precisely equal to the frequency of burst oscillations (van der Klis 2000), which are believed to match the spin frequency of the star. Most interestingly, kHz QPOs have recently been detected in an accreting millisecond pulsar, SAX J1808.4–3658, whose spin frequency is known (Wijnands et al. 2003). The $\sim$ 195-Hz frequency difference between the two kHz QPOs in this source is far below the 401-Hz spin frequency of the neutron star, but is consistent with half the spin frequency. Wijnands et al. (2003) argue that their observations falsify the beat-frequency model and pose a severe challenge for all current models of the kHz QPOs (but see Lamb & Miller 2003).

Stella & Vietri (1998,1999) proposed that the QPOs may be interpreted in terms of fundamental frequencies of test particles in motion in the relativistic potential of a neutron star or a black hole. They identified individual QPO frequencies with the orbital, periastron precession and nodal precession frequencies of test particles and showed that some predicted scalings between the frequencies agree with observations (Stella & Vietri 1999; Stella, Vietri & Morsink 1999). In contrast to some versions of the beat frequency model, this model does not require a magnetic field anchored in the central star, and thus provides a natural explanation for why twin QPOs are seen in both neutron-star and black-hole systems. However, the fact that the frequency difference between twin kHz QPOs in neutron star systems is often of order the neutron star frequency has no simple explanation. Also, since the model explicitly invokes general relativistic effects, it cannot explain the continuity in QPO properties between neutron stars and black holes on the one hand and white dwarfs on the other (Warner et al. 2003).

A number of scientists have investigated modes of oscillation of an accretion disk as a model of high frequency QPOs (for reviews see Kato, Fukue, & Mineshige 1998; Wagoner 1999; Kato 2001a). In an important paper, Okazaki, Kato, & Fukue (1987) showed that axisymmetric g-modes are trapped in the inner regions of a relativistic disk, where the epicyclic frequency κ reaches a maximum. This idea was exploited by Nowak & Wagoner (1991, 1992) and a number of other workers (Perez et al. 1997; Nowak et al. 1997; Silbergleit et al. 2001; Wagoner, Silbergleit, & Ortega-Rodriguez 2001; Abramowicz & Kluzniak 2001) who worked out the physical properties of the trapped modes. Much of the work has focused on neutral (i.e., non-growing) modes. The idea in such models is that, although the modes are stable, they might nevertheless be excited by some driving mechanism such as disk turbulence to produce the observed QPOs.

Recently, Kato (2001b, 2002) claimed to find that nonaxisymmetric g-modes are trapped

between two forbidden zones that lie on either side of the corotation radius and that the modes are highly unstable. Such dynamically unstable modes are very interesting since they would be self-excited and would spontaneously grow to non-linear amplitudes without the need for an external driving mechanism. Motivated by Kato's work, Li, Goodman, & Narayan (2003) studied nonaxisymmetric g-mode and p-mode instabilities in an unmagnetized isothermal accretion disk. They found that g- and p-modes with a nonzero number of vertical nodes are strongly absorbed at corotation and thus not amplified. Waves without vertical nodes are amplified (as known earlier, see Papaloizou & Pringle 1985; Goldreich, Goodman, & Narayan 1986; Narayan, Goldreich, & Goodman 1987), but the amplification is very weak. Therefore, any energy loss, either during propagation of the wave or during reflection at the boundaries, would kill the instability. Thus, Li et al. (2003) concluded, in agreement with Kato (2003), that nonaxisymmetric disk modes are not sufficiently unstable to be of interest for the QPO problem. Ortega-Rodriguez & Wagoner (2000) found that viscosity causes the fundamental g- and p-modes in a disk to grow, though the relevance of their result for QPOs is presently unclear.

Since the amplitude of intensity fluctuations observed in QPOs is often quite large, it is the opinion of the present authors that the oscillations are likely to be the result of a strongly-growing *instability* of some sort in the accretion flow. Having argued above that a hydrodynamic instability is ruled out (Kato 2003; Li et al. 2003), it is natural to consider the effect of magnetic fields via a magnetohydrodynamic (MHD) instability. Since, in general, only a small number of frequencies dominate the intensity fluctuations, the instability cannot be present at all disk radii (as in the case of the magnetorotational instability, Balbus & Hawley 1998), but must be associated with some special radius in the disk. The most natural choice for the special radius is the inner edge of the disk. Motivated by these arguments, we consider in this paper an accretion disk that is terminated at its inner edge by a strong vertical magnetic field. The resulting magnetospheric interface suffers from both the Rayleigh-Taylor and Kelvin-Helmholtz instabilities. We calculate the frequencies and growth rates of the unstable modes and consider the role that these modes play in the kHz QPOs seen in X-ray binaries.

The Rayleigh-Taylor instability and the related interchange instability have been considered by a number of authors, both for modeling QPOs (Titarchuk 2002, 2003) and in connection with other applications (Arons & Lea 1976a,b; Elsner & Lamb 1976, 1977; Michel 1977a,b; Spruit & Taam 1990; Kaisig, Tajima & Lovelace 1992; Lubow & Spruit 1995; Spruit, Stehle & Papaloizou 1995; Chandran 2001). We compare our work to these earlier studies.

The plan of the paper is as follows. In §2 we describe the model and its initial equilibrium state. In §3 we consider linear perturbations, derive a wave equation satisfied by

the perturbations, and obtain the corresponding jump conditions across the magnetospheric radius where there is a discontinuity in disk properties. In §4 we consider the case when the mass density of the disk has a jump but the angular velocity is continuous across the boundary; this situation occurs when the central object is a black hole. We show that, under suitable conditions, there is a Rayleigh-Taylor instability at the boundary, and we study in detail the growth of the instability using both analytical and numerical methods. In §5 we study the case when both the mass density and the angular velocity of the disk are discontinuous at the boundary, which corresponds to the situation when the central object is a neutron star. We show that both the Rayleigh-Taylor and the Kelvin-Helmholtz instabilities are present under suitable conditions. In §6 we summarize and discuss the results, and briefly compare the predictions of the model to observations of QPOs. In Appendix A we derive a necessary condition for disk instability. In Appendix B we briefly review classical results on the Rayleigh-Taylor and Kelvin-Helmholtz instabilities in Cartesian flows.

2. Basic Model and Initial Equilibrium

2.1. Outline of the Model

We consider a differentially-rotating axisymmetric accretion flow that is terminated on the inside by a strong magnetic field. The interface between the disk and the magnetosphere occurs at the magnetospheric radius r_m. The density experiences a jump at r_m, being larger on the outside and smaller on the inside. There may also be a jump in the angular velocity. Because of the density and velocity jumps, the system is potentially Rayleigh-Taylor and Kelvin-Helmholtz unstable (Chandrasekhar 1961; Drazin & Reid 1981).

The geometry we envisage is natural for accretion onto a magnetized neutron star. This geometry has been studied for many years (e.g., Ghosh & Lamb 1978, 1979) and there are several discussions of possible instabilities at the disk-magnetosphere interface (Arons & Lea 1976a,b; Elsner & Lamb 1976, 1977; Michel 1977a,b; Ikhsanov & Pustil'nik 1996). It has been suggested that the interchange instability (i.e., the Rayleigh-Taylor instability in the presence of magnetic fields) is the fastest mode of mass transport into the magnetosphere of an accreting magnetized neutron star (Elsner & Lamb 1984). When the accretion flow is spherical and the neutron star rotates slowly, the instability criterion is determined by a competition between the gravitational force of the neutron star and the poloidal curvature force of the magnetic field: gravity tends to drive the Rayleigh-Taylor instability, while the curvature force tends to stabilize the configuration (Arons & Lea 1976a,b; Elsner & Lamb 1976, 1977; Michel 1977a,b). When the neutron star rotates fast enough, the magnetospheric boundary becomes stable with respect to the interchange instability because of the

strong toroidal magnetic field that is produced in the boundary layer by the rotation of the magnetosphere relative to the spherical accretion flow (Ikhsanov & Pustil'nik 1996).

Similar processes for a thin Keplerian disk accreting onto a magnetized neutron star have been analysed by Spruit & Taam (1990). These authors confirmed that the Rayleigh-Taylor instability can be very effective in transporting mass across field lines, allowing the gas to drift along the midplane in a disk-like fashion even in regions of the magnetosphere that corotate with the central star. The interchange instability in a general thin accretion disk with differential rotation has been studied by Lubow & Spruit (1995) and Spruit et al. (1995). They found that disk shear tends to stabilize the configuration.

The model we consider differs from the studies cited above in one important respect: we explicitly avoid field curvature and focus on the pure Rayleigh-Taylor and Kelvin-Helmholtz problem for a disk-magnetosphere interface. The model is thus highly simplified and is perhaps most relevant for gas in the mid-plane of the accretion disk. We also ignore the toroidal component of the magnetic field, even though it may often be important (Ghosh & Lamb 1978; Ikhsanov & Pustil'nik 1996). A toroidal magnetic field affects the stability of the disk in two ways: (1) The toroidal field causes an inward force because of its curvature, enhancing the effective gravity in the disk and thereby boosting the Rayleigh-Taylor instability. (2) The toroidal magnetic field also produces a tension at the interface which tends to stabilize the disk (see, e.g, Chandrasekhar 1961). The overall effect will be determined by the competition between these two tendencies. We expect that for modes with a low azimuthal wave number the two effects will approximately cancel each other so that, at least for modest levels of toroidal field, the results may not be affected significantly. However, for modes with a large azimuthal wave number, the second effect will be dominant and so a toroidal field will very likely stabilize the disk.

Although our model is clearly relevant for neutron star accretion, it is in fact relevant also for accretion onto a black hole or an unmagnetized neutron star. Bisnovatyi-Kogan & Ruzmaikin (1974, 1976) proposed that an accretion flow around a black hole may, under certain circumstances, advect a considerable amount of magnetic flux to the center. Once enough magnetic flux has collected, the accumulated field will disrupt the flow at a magnetospheric radius, exactly as in our model. This idea has been confirmed in recent three-dimensional MHD simulations of radiatively inefficient accretion flows by Igumenshchev, Narayan, & Abramowicz (2003), and some additional consequences have been explored by Narayan, Igumenshchev & Abramowicz (2003). Something like a magnetosphere may also result from a global poloidal magnetic field being generated within the disk (Livio, Pringle, & King 2003).

The angular velocity profile has some important qualitative differences between the black hole and neutron star problems. In the black hole case, we expect the angular velocity

to be continuous across r_m (§4, Fig. 2), whereas in the neutron star case the angular velocity will in general be discontinuous at r_m (§5, Fig. 7). Thus, the disk-magnetosphere interface in the case of a black hole experiences only the Rayleigh-Taylor instability, whereas in the case of a neutron star it can have both the Rayleigh-Taylor and Kelvin-Helmholtz instabilities.

In order to be able to handle both the black hole and neutron star problems, we set up the theoretical framework sufficiently generally as far as the angular velocity profile is concerned. However, to make the analysis tractable, we make some other drastic simplifications. First, we assume that the gas is incompressible. With this approximation, compressive waves are filtered out. The interchange and Kelvin-Helmholtz instabilities, which are our main interest and which are both incompressible in nature, survive unaffected (Spruit et al. 1995). Second, we assume that the magnetic field is purely along the z-axis (i.e., parallel to the rotation axis of the gas flow) and that all fluid quantities are independent of z. We thus solve a cylindrically symmetric problem in which $\partial/\partial z = 0$ and all quantities are function only of the cylindrical radius r and the azimuthal angle ϕ. The geometry of the model is as shown in Figure 1.

We describe below in §2.2 the equilibrium flow, and analyse in §3 the effect of linear perturbations.

2.2. Basic Equations and the Initial Equilibrium State

The dynamics of a perfectly conducting and magnetized Newtonian accretion disk is governed by the basic equations of MHD (Balbus & Hawley 1998, we neglect viscosity and resistivity):

$$\frac{\partial \rho}{\partial t} + \nabla \cdot (\rho \mathbf{v}) = 0 \,, \tag{1}$$

$$\rho \left(\frac{\partial}{\partial t} + \mathbf{v} \cdot \nabla \right) \mathbf{v} = -\rho \nabla \Phi - \nabla \left(p + \frac{B^2}{8\pi} \right) + \frac{1}{4\pi} \mathbf{B} \cdot \nabla \mathbf{B} \,, \tag{2}$$

$$\frac{\partial \mathbf{B}}{\partial t} = \nabla \times (\mathbf{v} \times \mathbf{B}) \,, \tag{3}$$

$$\nabla \cdot \mathbf{B} = 0 \,, \tag{4}$$

where ρ is the mass density, $\mathbf{v}$ is the velocity, Φ is the gravitational potential of the central compact object, p is the gas pressure, and $\mathbf{B}$ is the magnetic field. Equations (1)–(3) are respectively the continuity, momentum and induction equations, and equation (4) is one of Maxwell equations.

We assume that the disk fluid is incompressible, i.e.

$$\nabla \cdot \mathbf{v} = 0 \ . \tag{5}$$

Substituting this in the continuity equation (1) gives

$$\frac{d\rho}{dt} = 0 \ , \qquad \frac{d}{dt} \equiv \frac{\partial}{\partial t} + \mathbf{v} \cdot \nabla \ , \tag{6}$$

where d/dt is the Lagrangian time derivative as measured in the comoving frame of the fluid. Equation (6) states that the mass density measured by a comoving observer does not change with time, which is obvious for an incompressible fluid.

As explained in §2.1, the equilibrium state is assumed to be described by

$$\rho = \rho_0(r) \ , \qquad p = p_0(r) \ , \qquad \mathbf{v} = \Omega(r) r \, \mathbf{e}_\phi \ , \qquad \mathbf{B} = B_0(r) \, \mathbf{e}_z \ , \tag{7}$$

where $\mathbf{e}_i$ $(i = r, \phi, z)$ are unit coordinate vectors, and we use the subscript 0 to refer to the equilibrium. Equations (1), (3)–(6) are automatically satisfied by such an equilibrium, while equation (2) gives an additional requirement:

$$g_{\rm eff} = -\frac{1}{\rho_0} \frac{dp_{t0}}{dr} \ . \tag{8}$$

Here, the effective gravitational acceleration $g_{\rm eff}$ and the associated frequency $\Omega_{\rm eff}$ are defined by

$$g_{\rm eff} \equiv \Omega_{\rm eff}^2 r = \frac{d\Phi}{dr} - \Omega^2 r \ , \tag{9}$$

and the total pressure p_t is given by

$$p_t \equiv p + \frac{B^2}{8\pi} \ . \tag{10}$$

Equation (8) states that the net radial force, obtained by summing the gravitational, centrifugal and (total) pressure gradient forces, vanishes in equilibrium. Note that, to be consistent with the assumption of cylindrical symmetry, the background gravitational potential Φ must be a function of only the cylindrical radius r. This is one of the many simplifications we have made in the model.

As explained in §2.1, the initial equilibrium consists of two distinct zones separated at a radius r_m (Fig. 1). At r_m, there is a discontinuity in ρ and $\mathbf{B}$, and sometimes also in Ω and $\mathbf{v}$ (see §5 below). However, the pressure p is always continuous.

3. Linear Perturbations

3.1. Wave Equation

We now consider linear perturbations of the equilibrium configuration. We take the perturbations to be proportional to $\exp[i(-\omega t+m\phi)]$, where ω is the mode frequency, which is in general complex, and m is the number of nodes in the ϕ direction; the azimuthal wavevector is equal to m/r. We assume that the perturbations are independent of z. Therefore, magnetic field lines which are initially parallel to z (by assumption) remain so even in the perturbed state, and the r- and ϕ-components of the magnetic field vanish at all times. We then have from equation (2),

$$\mathbf{B}\cdot\nabla \propto \frac{\partial}{\partial z} = 0 \; . \tag{11}$$

Since we have further assumed that the gravitational potential Φ is a function only of r, none of the force terms on the right-hand side of equation (2) has a vertical component. Therefore, the vertical velocity perturbation is also zero. The linear perturbations to the mass density, gas pressure, velocity, and magnetic field may be written as

$$\left\{ \begin{array}{c} \delta\rho \\ \delta p \\ \delta\mathbf{v} \\ \delta\mathbf{B} \end{array} \right\} = \left\{ \begin{array}{c} \rho_1(r) \\ p_1(r) \\ u(r)\,\mathbf{e}_r + v(r)\,\mathbf{e}_\phi \\ B_1(r)\,\mathbf{e}_z \end{array} \right\} \times e^{-i\omega t+im\phi} \; . \tag{12}$$

Taking the curl of equation (2) and substituting equations (5) and (11) gives the following equation for the vorticity,

$$\frac{d}{dt}\left(\nabla\times\mathbf{v}\right) = -\frac{1}{\rho}\nabla\rho\times\left(\nabla\Phi+\frac{d\mathbf{v}}{dt}\right) \; . \tag{13}$$

Equations (5), (6), and (13) then form a complete set of equations for $\mathbf{v}$ and ρ. These equations are independent of the gas pressure and the magnetic field. The first order perturbations of equations (5) and (6) give

$$\frac{1}{r}\frac{d}{dr}(ru)+\frac{im}{r}\,v = 0 \; , \tag{14}$$

$$i\sigma\rho_1 - u\,\frac{d\rho_0}{dr} = 0 \; , \tag{15}$$

respectively, where

$$\sigma \equiv \omega - m\Omega \; . \tag{16}$$

Similarly, the first order perturbation of equation (13) gives

$$\frac{1}{r\rho_0}\frac{d}{dr}\left(r\rho_0 v\right) + \left[\frac{i}{\sigma\rho_0}\frac{d}{dr}\left(\frac{\rho_0\kappa^2}{2\Omega}\right) - \frac{im}{r}\right]u = \frac{\rho_1}{\rho_0}\frac{mg_{\rm eff}}{r\sigma}\ , \tag{17}$$

where the epicyclic frequency κ and the related vorticity frequency ζ are defined by

$$\frac{\kappa^2}{2\Omega} \equiv \frac{1}{r}\frac{d}{dr}(r^2\Omega) \equiv 2\zeta\ . \tag{18}$$

Finally, from equations (14), (15), and (17), a wave equation can be derived for the quantity $W \equiv ru$:

$$\frac{1}{r\rho_0}\frac{d}{dr}\left(r\rho_0\frac{dW}{dr}\right) - \frac{m^2}{r^2}\left[\frac{\Omega_{\rm eff}^2}{\sigma^2}\frac{d\ln\rho_0}{d\ln r} - \frac{2\zeta}{m\sigma}\frac{d\ln\left(\rho_0\zeta\right)}{d\ln r} + 1\right]W = 0\ . \tag{19}$$

This is the fundamental equation for the model considered in this paper. The mode frequency ω is an eigenvalue of this second order differential equation and is determined by solving the equation and applying the boundary conditions. Any eigenvalue ω with a positive imaginary part represents an unstable mode. We focus on such modes in the rest of the paper. It is possible to derive a necessary condition for the existence of instability, as shown in Appendix A, but we do not use that condition in the main paper.

Once the eigenvalue ω and the eigenfunction $W \equiv ru$ are obtained, we may solve for the other perturbed quantities by going back to the linear perturbation equations. Thus, equation (14) gives the perturbed azimuthal velocity $v(r)$, and equation (15) gives the perturbed density $\rho_1(r)$. To calculate the perturbed total pressure $p_{t1}(r)$, we use the azimuthal component of the first order perturbation of the momentum equation (2),

$$2\zeta u - i\sigma v = -\frac{im}{r}\frac{p_{t1}}{\rho_0}\ . \tag{20}$$

The perturbed magnetic field B_1 can be calculated from the first order perturbation of the induction equation (3),

$$B_1 = -\frac{i}{\sigma}\frac{dB_0}{dr}u\ , \tag{21}$$

where equation (14) has been substituted. Finally, the perturbed gas pressure p_1 can be calculated from equations (20) and (21), by making use of $p_1 = p_{t1} - B_0B_1/4\pi$.

3.2. Jump Conditions Across the Boundary

Since the equilibrium model has a discontinuity at $r = r_m$, where the accretion disk meets the magnetosphere, the solution must satisfy certain junction conditions at this boundary. Let us define $r_{m+} \equiv r_m + 0^+$ and $r_{m-} \equiv r_m + 0^-$ as the radius r_m on the two sides of

the boundary. Let us also define $\Delta_m(f)$ to denote the jump in the value of any quantity f across the boundary, i.e.

$$\Delta_m(f) \equiv f\left(r_{m+}\right) - f\left(r_{m-}\right) \ . \tag{22}$$

Consider first the Lagrangian displacement in the radial direction: $\xi = iu/\sigma$. Clearly, the displacement has to be the same on the two sides of the boundary. This gives the first jump condition:

$$\Delta_m \left(\frac{W}{\sigma}\right) = 0 \ . \tag{23}$$

Since σ is in general not continuous at $r = r_m$ (because Ω need not be continuous), note that it is the quantity W/σ that is continuous at the boundary, while W itself may or may not be continuous, depending on the behavior of Ω.

Consider next the total Lagrangian pressure perturbation at the displaced position of the fluid:

$$p_{t1,\mathrm{L}} = p_{t1} + \xi \frac{dp_{t0}}{dr} = p_{t1} - \xi \rho_0 g_{\mathrm{eff}} \ , \tag{24}$$

where we have used equation (8) in the last step. We may rewrite p_{t1} in terms of u and v using equation (20) and then replace these in terms of W and dW/dr. Carrying out these steps, and requiring the Lagrangian pressure perturbation to be equal on the two sides of the boundary, we obtain the second jump condition:

$$\Delta_m \left[\sigma \rho_0 \frac{dW}{dr} - \frac{m}{r}\left(\frac{m\Omega_{\mathrm{eff}}^2}{\sigma} - 2\zeta\right)\rho_0 W\right] = 0 \ . \tag{25}$$

The two jump conditions (23) and (25) form a complete set of relations that must be satisfied at $r = r_m$.

4. Models with Continuous Ω at the Interface

We first consider a model in which the angular velocity is continuous across r_m, and take the profile of Ω to be given by (see Fig. 2)

$$\Omega(r) = \Omega_m \left(\frac{r}{r_m}\right)^{-q} \ . \tag{26}$$

The corresponding vorticity frequency is

$$\zeta(r) = \left(1 - \frac{q}{2}\right) \Omega(r) \ . \tag{27}$$

For completeness, we consider values of the index q over the range from 0 (constant angular velocity) to 2 (constant specific angular momentum). However, in real accretion disks, the relevant range is likely to be from 3/2 (Keplerian) to 2. We assume that the gravitational potential $\Phi \propto r^{-1}$.

A model with continuous Ω is not likely to be relevant for accreting neutron stars, since we expect in general a discontinuity in Ω at the interface between the disk and the magnetosphere. However, in the case of accretion onto a magnetosphere surrounding a black hole, since the field is not anchored to the black hole, we expect the magnetospheric fluid to corotate with the surrounding disk. Thus, the discussion in this section is most relevant for the black hole case. It is possible that the value of q may change across the boundary for a real black hole flow. We do not consider this possibility here, though the equations we write are general enough to handle it.[2]

As described in §2.1, we assume that there is a density jump at r_m. Thus, we model the density profile as

$$\rho_0 = \begin{cases} \rho_- \ , & \text{if } r < r_m \\ \rho_+ (r/r_m)^{-\gamma} \ , & \text{if } r > r_m \end{cases} \ , \tag{28}$$

where ρ_+, ρ_-, and γ are constants. When $\gamma > 0$, the mass density decays with increasing radius for $r > r_m$. The jump in mass density at r_m is described by the following dimensionless parameter,

$$\mu \equiv \frac{\rho_+ - \rho_-}{\rho_+ + \rho_-} \ . \tag{29}$$

Note that μ can in general take any value between -1 and $+1$. However, we only consider values of $\mu > 0$, i.e., $\rho_+ > \rho_-$.

Because Ω is continuous at r_m, so is σ. Therefore, the two jump conditions written in §3.2 become simplified to

$$\Delta_m(W) = 0 \ , \tag{30}$$

[2]Neglecting a possible change in q across the boundary is reasonable especially when the following fact is considered: when the disk has a sharp contrast in mass density across the boundary (i.e., $\rho_+ \gg \rho_-$), the solutions do not depend on the details of the disk inside $r = r_m$.

$$\Delta_m \left(\rho_0 \frac{dW}{dr} \right) = \left[\frac{m^2 \Omega_{\rm eff}^2}{\sigma^2} - \frac{2m\zeta}{\sigma} \right]_{r=r_m} \frac{W_m}{r_m} \, \Delta_m(\rho_0) \ . \tag{31}$$

The former equation states that W is continuous at r_m. We write the value of W at this radius as W_m. In the latter equation, $\rho_0 = \rho_+$ for $r = r_{m+}$ and ρ_- for $r = r_{m-}$.

4.1. Analytical Results

We start first with the simplest case: (1) We assume that $\gamma = 0$, i.e., the mass density is constant on the two sides of the boundary, with a jump at the junction described by the parameter μ. (2) We assume that q is equal to either 0 or 2.

The first assumption implies that the term involving $d \ln \rho_0 / d \ln r$ in equation (19) vanishes, while the second assumption means that the term involving $d \ln(\rho_0 \zeta) / d \ln r$ vanishes, either because ζ is constant (for $q = 0$) or it is equal to 0 (for $q = 2$). Therefore, away from the boundary $r = r_m$, the wave equation (19) takes the form

$$\frac{1}{r} \frac{d}{dr} \left(r \frac{dW}{dr} \right) - \frac{m^2}{r^2} = 0 \ . \tag{32}$$

This differential equation has two simple solutions: $W \propto r^{+m}$, r^{-m}. We require the perturbations to decay away from the boundary, both as $r \to \infty$ and as $r \to 0$. Therefore, for $m \geq 1$, the solution must be of the form

$$W = \begin{cases} A_- r^m \ , & \text{if } r < r_m \\ A_+ r^{-m} \ , & \text{if } r > r_m \end{cases} \ , \tag{33}$$

where A_+ and A_- are constants.

We now apply the two jump conditions (30) and (31). Since $\Delta_m(W) = 0$, we must have

$$A_+ = A_- r_m^{2m} \ . \tag{34}$$

Thus,

$$\Delta_m \left(\rho_0 \frac{dW}{dr} \right) = - \left(\rho_+ + \rho_- \right) m A_- r_m^{m-1} \ . \tag{35}$$

Applying this to the second jump condition (31), we obtain a solution for the eigenvalue $\omega = \sigma + m\Omega$,

$$\omega = \left[m\Omega + \mu\zeta \pm \sqrt{-\mu m \Omega_{\rm eff}^2 + \mu^2 \zeta^2} \right]_{r=r_m} \ , \qquad q = 0, \ 2 \ , \tag{36}$$

where μ is the density contrast parameter defined in equation (29).

We are interested in unstable modes, i.e., modes with complex ω, where the growth rate of the instability is given by $\omega_{\rm I}$. From equation (36), we see that unstable modes exist whenever $-\mu m\Omega_{\rm eff}^2 + \mu^2\zeta^2 < 0$, i.e. if

$$0 < \mu < \mu_1 \ , \qquad \mu_1 \equiv \left.\frac{m\Omega_{\rm eff}^2}{\zeta^2}\right|_{r=r_m} > 0 \ . \tag{37}$$

Thus, the instability exists only if μ is positive, i.e., if the density on the outside is greater than that on the inside. This is perfectly natural for the Rayleigh-Taylor instability. Surprisingly, if the density contrast is too large, i.e., if $\mu > \mu_1$, the instability shuts off. This is clearly the result of rotation, or more specifically vorticity. When $q = 2$ and the vorticity $\zeta = 0$, then $\mu_1 \to \infty$, and the instability is present for any positive value of μ. However, for $q = 0$, we have $\zeta = \Omega$ and μ_1 is finite. In this case, if $\Omega_{\rm eff}^2$ small (i.e., the effective gravity is weak) and if we consider a low value of the azimuthal wavenumber m, the vorticity is able to eliminate the instability.

The real part of ω gives the observed oscillation frequency of the mode. When $q = 2$, this is simply equal to $m\Omega_m$. In this case, the mode is stationary in the frame of the fluid at the boundary, and what one observes is simply the Keplerian frequency Ω_m of the gas at the inner edge of the disk. However, when $q = 0$, the observed mode frequency is not equal to $m\Omega_m$, but is equal to $(m + \mu)\Omega_m$, which differs from the orbital frequency. In this case, because of vorticity, we have a traveling mode in the fluid frame.

4.2. Numerical Results

For a more general disk, with $\gamma \neq 0$ and/or $q \neq 0, 2$, we have to solve the wave equation and the boundary conditions numerically. Although we derived in §3.1 a second-order differential equation as our basic wave equation (eq. [19]), for numerical purposes a pair of equivalent first-order differential equations is more convenient. Defining $V = rv$, we write

$$\frac{d}{dr}\left\{\begin{array}{c} W \\ V \end{array}\right\} = \left\{\begin{array}{cc} 0 & -\frac{im}{r} \\ \frac{im}{r}\left[1 - \frac{2r}{m\sigma}\frac{d\zeta}{dr} + \left(\frac{\Omega_{\rm eff}^2}{\sigma^2} - \frac{2\zeta}{m\sigma}\right)\frac{r}{\rho_0}\frac{d\rho_0}{dr}\right] & -\frac{1}{\rho_0}\frac{d\rho_0}{dr} \end{array}\right\}\left\{\begin{array}{c} W \\ V \end{array}\right\} . \tag{38}$$

The first jump condition at $r = r_m$ is that W must be continuous (eq. [30]). From equations (31) and (14), we have

$$\Delta_m(\rho_0 V) = i\left[\frac{m\Omega_{\rm eff}^2}{\sigma^2} - \frac{2\zeta}{\sigma}\right]_{r=r_m} W_m\, \Delta_m\rho_0 \ , \tag{39}$$

where $W_m = W(r_m)$. Substituting equation (29) into this, we obtain the second jump condition

$$(1+\mu)V_+ - (1-\mu)V_- = 2i\left[\frac{m\Omega_{\rm eff}^2}{\sigma^2} - \frac{2\zeta}{\sigma}\right]_{r=r_m} W_m\,\mu\ . \tag{40}$$

We integrate the two first-order equations (38) from a small radius $r = r_1 \ll r_m$ outward, and simultaneously also from a large radius $r = r_2 \gg r_m$ inward. Where the two integrations meet at $r = r_m$, we adjust the relative normalization factor and the eigenvalue ω such that the two jump conditions are satisfied. The starting values of W and V at $r = r_1$ and r_2 are chosen to correspond to the appropriate eigenvectors of the operator d/dr in equation (38). At $r = r_1$, we require that the real part of the eigenvalue should be positive, so that $d|W|^2/dr > 0$ and $d|V|^2/dr > 0$, while at $r = r_2$, we require that the real part of the eigenvalue should be negative, so that $d|W|^2/dr < 0$ and $d|V|^2/dr < 0$. The two eigenvalues of d/dr (see eq. [38]) are

$$k_{1,2} = \frac{1}{2}\left\{-\frac{1}{\rho_0}\frac{d\rho_0}{dr} \pm \sqrt{\left(\frac{1}{\rho_0}\frac{d\rho_0}{dr}\right)^2 + \frac{4m^2}{r^2}\left[1 - \frac{2r}{m\sigma}\frac{d\zeta}{dr} + \left(\frac{\Omega_{\rm eff}^2}{\sigma^2} - \frac{2\zeta}{m\sigma}\right)\frac{r}{\rho_0}\frac{d\rho_0}{dr}\right]}\right\}\ . \tag{41}$$

The corresponding two eigenvectors (up to a normalization factor) are, respectively,

$$\left\{\begin{array}{c} W \\ V \end{array}\right\}_1 = \left\{\begin{array}{c} 1 \\ \frac{ir}{m}k_1 \end{array}\right\}\ , \qquad \left\{\begin{array}{c} W \\ V \end{array}\right\}_2 = \left\{\begin{array}{c} 1 \\ \frac{ir}{m}k_2 \end{array}\right\}\ . \tag{42}$$

It can be checked that, at both $r = r_1 \ll r_m$ and $r = r_2 \gg r_m$, k_1 is positive and k_2 is negative. Therefore, the eigenvector corresponding to k_1 is a physical solution at $r = r_1$, and the eigenvector corresponding to k_2 is a physical solution at $r = r_2$. Thus, in our numerical calculations, we choose $W = r_1^m$ and $V = ir_1^{m+1}k_1(r_1)/m$ at $r = r_1$, and $W = r_2^{-m}$ and $V = ir_2^{-m+1}k_2(r_2)/m$ at $r = r_2$, as the starting values of W and V.

One comment is in order regarding the integration. The point $\sigma = 0$ is a singularity of equation (38); it represents the corotation singularity. Therefore, while integrating the equation numerically, it is important to make sure that the integration contour goes above the singularity (Narayan, Goldreich, & Goodman 1987). When ω (thus σ) is complex, this is easily arranged by just integrating along the real r-axis since the singularity is below the real axis for positive $\omega_{\rm I}$ (which corresponds to an unstable mode, recall our convention that the perturbations are $\propto \exp[-i\omega t]$). However, when ω is real, the corotation singularity is on the real r-axis. In this case, the integration contour must go above the singularity in the complex r-plane.

We present some numerical results in Figs. 3–6. In Figure 3, we show the frequency $\omega = \omega_{\rm R} + i\omega_{\rm I}$, in units of $\Omega_m = \Omega(r_m)$, corresponding to a model with $\mu = 1$, $\Omega^2_{{\rm eff},m} = 0.6\Omega^2_m$, and $\gamma = 0$ (i.e., constant mass density away from $r = r_m$). The solid lines show $\omega_{\rm I}$ and give the growth rate of unstable modes. The dashed lines represent $\omega_{\rm R}$, and correspond to the observed oscillation frequency of the mode. The results are perfectly reasonable — mode frequencies vary smoothly as a function of q between the two limits $q = 0$ and $q = 2$ (where we have analytical results, §4.1). For $m = 1$ and small values of q, we see that the instability shuts off and we have instead two neutral modes with real ω. This is not unexpected. The analytical results in §4.1 indicate that for $q = 0$ and this set of parameters, we have $\mu > \mu_1$, which indicates that there should be no instability.

For the parameters used in Fig. 3 and for q in the range 1.5–2 of interest for accretion disks, we find that all azimuthal wave numbers m are unstable. However, as equation (37) shows, whether or not a given mode is stable or unstable depends on whether μ is greater than or less than μ_1 and this depends on the magnitude of $\Omega^2_{\rm eff}/\zeta^2$. (Although the result given in eq. [37] is true only for $q = 0,\ 2$, the qualitative result is valid also for other values of q.) In Figure 4 we show the numerically determined critical values of $\Omega^2_{{\rm eff},m}$ that separate stable and unstable modes in the $q - \Omega^2_{{\rm eff},m}$ plane (we restrict our attention to q in the range 1.5–2 which is of most interest for QPOs). The results correspond to $\mu = 1$, $\gamma = 0$. We see that, for $q < 2$, there always exists a range of $\Omega^2_{{\rm eff},m}$ over which modes with a given m are stable. For example, when $q = 1.5$ and $0.024 < \Omega^2_{{\rm eff},m}/\Omega^2_m < 0.04$, modes with $m = 1$ are stable and modes with $m \geq 2$ are unstable, while for $0.018 < \Omega^2_{{\rm eff},m}/\Omega^2_m < 0.024$, modes with $m \leq 2$ are stable and modes with $m \geq 3$ are unstable.

Figure 5 shows results for some other choices of parameters: $\mu = 0.8$, $\Omega^2_{{\rm eff},m} = \Omega^2_m$, and $\gamma = 0$ in panel (a); $\mu = 1$, $\Omega^2_{{\rm eff},m} = \Omega^2_m$, and $\gamma = 0$ in panel (b); and, $\mu = 1$, $\Omega^2_{{\rm eff},m} = \Omega^2_m$, and $\gamma = 1$ in panel (c). Comparing panel (b) with Figure 3, we see that the zone of stable modes at small q and $m = 1$ seen in the latter, disappears when $\Omega^2_{\rm eff}$ increases. This is because μ_1 increases and becomes larger than μ. All other features are very similar. Comparing panels (a) and (b) of Figure 5, we see the effect of varying μ. For this particular set of parameters, for $m = 1$ we see that $\omega_{\rm I}$ decreases with increasing μ when q is close to 0, but increases with increasing μ when q is close to 2. For $m > 1$, however, $\omega_{\rm I}$ always increases with increasing μ. The real part of the frequency, $\omega_{\rm R}$, increases with increasing μ for $0 \leq q < 2$, but remains independent of μ for $q = 2$ (see eq. [36]). Finally, by comparing panels (b) and (c), we see the effect of having a non-constant density ($\gamma \neq 0$). Generally, as γ increases, $\omega_{\rm I}$ also increases, but $\omega_{\rm R}$ is hardly affected.

In Figure 6 we show results corresponding to a Keplerian-type disk ($q = 3/2$), as a function of μ, for $\Omega^2_{{\rm eff},m} = 0.2\Omega^2_m$ and $\gamma = 1$ (i.e., the mass density decays with increasing

radius according to $\rho \propto r^{-1}$). We see that the imaginary part of the frequency $\omega_{\rm I}$ strongly depends on μ, with $\omega_{\rm I} \to 0$ as $\mu \to 0$. This is because the instability is driven by the density contrast at the boundary. As the density contrast goes to zero, the instability must clearly vanish. The real part of the frequency, $\omega_{\rm R}$, however, depends only weakly on μ.

Summarizing, we find that the Rayleigh-Taylor instability operates over a wide range of parameters so long as the density on the outside is greater than the density on the inside. The growth rate of the instability is typically large, of order $\sim \Omega_{\rm eff}$, which means that the growth occurs fairly rapidly. For $3/2 \leq q \leq 2$, the range of interest for accretion disks, the real part of the frequency is nearly equal to $m\Omega_m$ in almost all cases. This is because the mode nearly corotates with the gas at r_m. For a large density contrast $\mu \to 1$ and a weak effective gravity $\Omega_{\rm eff}^2 \ll \Omega_m^2$, low-$m$ modes become stable and the instability is limited to higher-m modes.

5. Models with Discontinuous Ω at the Interface

We now consider a model that is more appropriate for an accretion flow around a magnetized neutron star (Ghosh & Lamb 1978, 1979). Since the magnetic field of a neutron star is frozen to the star, the low density plasma in the magnetosphere ($r < r_m$) must corotate rigidly with the star. However, outside the magnetospheric radius, we expect the accreting gas to rotate differentially as in a standard accretion disk. Also, the angular velocity of the disk at r_m will, in general, not match the angular velocity of the star. Based on these considerations, we assume the following model for the angular velocity (Fig. 7):

$$\Omega = \begin{cases} \Omega_- \,, & \text{if } r < r_m \\ \Omega_+ (r/r_m)^{-q} \,, & \text{if } r > r_m \end{cases} \,, \tag{43}$$

where Ω_+ and Ω_- are constants. In general $\Omega_- \neq \Omega_+$. For the density profile, we assume the same model as in equation (28).

The jump conditions are given by equations (23) and (25).

5.1. Analytical Results

As in §4.1, we consider the special case when $\gamma = 0$ and $q = 0$ or 2. We may then repeat the same steps described in §4.1, except that the jump conditions are now different. We obtain the following results for the eigenvalue,

$$\omega = \frac{1}{2}\left[(1+\mu)\,(m\Omega_+ + \zeta_+) + (1-\mu)\,(m\Omega_- - \zeta_-) \pm \sqrt{-\Theta}\right] \,, \tag{44}$$

where the "+" and the "−"in the subscripts denote evaluations at $r = r_{m+}$ and at $r = r_{m-}$, respectively, and

$$\begin{aligned}\Theta \equiv\ & 2\left[(1+\mu)\left(m\Omega_{\rm eff,+}^2 - \zeta_+^2\right) - (1-\mu)\left(m\Omega_{\rm eff,-}^2 + \zeta_-^2\right)\right] \\ & + \left(1-\mu^2\right)\left[m\left(\Omega_+ - \Omega_-\right) + \zeta_+ + \zeta_-\right]^2 \ . \end{aligned} \tag{45}$$

When $\Omega_+ = \Omega_-$ (which means $\zeta_+ = \zeta_-$, $\Omega_{\rm eff,+} = \Omega_{\rm eff,-}$), equation (44) simplifies to equation (36).

When Θ is positive, there is an instability. A study of the expression for Θ indicates that there are two distinct terms, written in separate lines in equation (45). Therefore, there are two distinct mechanisms of instability. The first term in (45) is the one we have already seen in §4, due to the Rayleigh-Taylor instability. If Ω and its derivative are continuous at r_m, this is the only term present, and it gives an instability only if $\rho_+ > \rho_-$, i.e., $\mu > 1$. However, for the problem at hand, Ω is discontinuous at r_m, and so the second term can also be important. Ignoring the vorticity terms $\zeta_\pm$ for simplicity, this term is directly proportional to $(\Omega_+ - \Omega_-)^2$, i.e., the square of the angular velocity jump across the boundary. This term is nothing but the classical Kelvin-Helmholtz instability associated with a velocity discontinuity.

The observed mode frequency is given by the real part of ω in equation (44). If $\mu = 1$, i.e., we have the maximum density contrast across the boundary, then the frequency is just equal to the appropriate frequency $m\Omega_+ + \zeta_+$ of the outer accretion disk at r_{m+}. That is, the rotation rate of the neutron star Ω_- is irrelevant. This is reasonable since there is no mass associated with the flow inside r_m, and so the frequency Ω_- of this region of the flow should have no influence on the mode. However, when $\mu \neq 1$, the mode frequency is a linear combination of $m\Omega_+ + \zeta_+$ and $m\Omega_- + \zeta_-$, with weights given by the two densities.

All of these results are very reminiscent of the classical results for the Rayleigh-Taylor and Kelvin-Helmholtz instability (Drazin & Reid 1981). We discuss this connection in Appendix B.

5.2. Numerical Results

For the general case with $\gamma \neq 0$ and/or $q \neq 0, 2$, we numerically solve equations (38), (23), and (46), following the numerical approach described in §4.1. We write the jump condition (25) as

$$\Delta_m \left[\sigma\rho_0 V - i\left(\frac{m\Omega_{\rm eff}^2}{\sigma} - 2\zeta\right)\rho_0 W\right] = 0 \ . \tag{46}$$

In Figure 8 we show some numerical results for a disk with $\gamma = 0$, $\mu = 0.4$ and the frequency of effective gravity $\Omega^2_{\rm eff,+} = \Omega^2_+$. In panel (a), the disk angular velocity satisfies $\Omega_- = 2\Omega_+$, i.e., the neutron star rotates twice as fast as the disk at $r = r_m$. In panel (b), the disk angular velocity satisfies $\Omega_- = \Omega_+$, i.e., the neutron star rotates at the same rate as the disk and the angular velocity is continuous (but not smooth) at $r = r_m$. In panel (c), the disk angular velocity satisfies $\Omega_- = 0.4\Omega_+$, i.e., the neutron star rotates more slowly than the disk.

Comparing the three panels, we see that the real part of the frequency ($\omega_{\rm R}$) monotonically decreases as Ω_-/Ω_+ decreases. This is as expected. Based on the discussion in §5.1, the mode frequency is a linear combination of the outer and inner frequencies at the boundary. As the latter decreases, the mode frequency must also decrease. The growth rate of the mode is more interesting; it is minimum when $\Omega_-/\Omega_+ = 1$, and increases both for $\Omega_-/\Omega_+ > 1$ and $\Omega_-/\Omega_+ < 1$. This behavior is because of the simultaneous presence of the Rayleigh-Taylor and Kelvin-Helmholtz instabilities. When $\Omega_-/\Omega_+ = 1$, there is no velocity discontinuity at the boundary and we have only the Rayleigh-Taylor instability, with a certain growth rate. However, both for $\Omega_-/\Omega_+ < 1$ and $\Omega_-/\Omega_+ > 1$, there is an additional contribution to the growth rate from the Kelvin-Helmholtz instability, and so the net growth rate is enhanced.

Note that, for the case shown in panel (a), we have $\Omega^2_{\rm eff,-} = -0.5\Omega^2_-$, indicating that the disk is super-Keplerian right inside $r = r_m$. But there are still unstable modes in this case, since the disk is sub-Keplerian for $r > r_m$. For the cases shown in panels (b) and (c), the disk is sub-Keplerian for both $r < r_m$ and $r > r_m$.

6. Summary and Discussion

The main message of this paper is that there are instabilities associated with the magnetospheric radius where an accretion disk meets the magnetosphere of the central mass and that these instabilities may be relevant for understanding QPOs in binary systems. There are two natural instabilities at the disk-magnetosphere interface: (1) Rayleigh-Taylor (or interchange) instability associated with a density jump, and (2) Kelvin-Helmholtz instability associated with an angular velocity jump. These instabilities, which are well-known for classical uniform Cartesian flows (Appendix B), survive with relatively little modification for a rotating, shearing flow with a density gradient (§§4,5). The unstable modes are expected to grow to become nonaxisymmetric perturbations with large amplitude (e.g., the streams in the simulations of Igumenshchev et al. 2003) and to give strong quasi-periodic variations in the observed intensity.

If, as we propose, these instabilities are responsible for the observed QPOs in X-ray binaries, the same model might work both for neutron stars and black holes. The existence of a disk-magnetosphere interface around accreting magnetized neutron stars is well-known. The popular beat frequency model for QPOs invokes blobs in the accretion disk orbiting at the Keplerian frequency at the magnetospheric radius (Alpar & Shaham 1985; Lamb et al. 1985; Strohmayer et al. 1996) or at the sonic radius (Miller, Lamb, & Psaltis 1998; Lamb & Miller 2001). While the model does not explain the origin of the blobs, it is reasonable to assume that the blobs are in some cases at least created by the interchange and Kelvin-Helmholtz instabilities studied in this paper. A fact not widely appreciated is that the magnetospheric model might also apply to accreting black holes and unmagnetized neutron stars. As Bisnovatyi-Kogan & Ruzmaikin (1976) showed, it is possible for the region close to a black hole to become magnetically dominant (Livio et al. 2003; Narayan et al. 2003). An accretion disk would then be disrupted at a magnetospheric radius, just as in the neutron star case, and the interface would be unstable and produce QPOs. The main difference between the two cases is that the magnetic field is not anchored to the black hole, and so the magnetosphere does not rotate rigidly with the star as in the neutron star case. This difference between the black hole and neutron star problems leads to some differences in the results for the two cases, as discussed in §§4,5.

Our analysis shows that nearly all azimuthal wavenumbers m are unstable under reasonable conditions. Although modes with higher values of m grow more rapidly, we expect that these modes will saturate at relatively small amplitudes. The low-m modes, on the other hand, are likely to grow to large amplitude and are therefore of most interest for understanding QPOs. For q in the range 3/2 to 2 (Keplerian to constant angular momentum), and reasonable assumptions about the density profile, we have shown that the observed mode frequency tends to be of order $m\Omega_m$. Thus, in the simplest version of the model, we expect the observed QPO frequencies to be in the ratio 1:2:3, etc. However, as we showed in §4 (see Fig. 4), it may often be the case that the $m = 1$ mode is stable and that only modes with $m \geq 2$ are unstable. This should happen whenever the effective gravity in the radial direction is weak, i.e., when the gas pressure in the disk is low. In this case, the QPO frequencies should be roughly in the ratio 2:3:4, etc. It is interesting that a frequency ratio 2:3 is frequently seen in both black hole and neutron star systems (Abramowicz & Kluzniak 2001; Abramowicz et al. 2003; Remillard et al. 2002a).

We have emphasized that, in our opinion, QPOs should be produced by the growing modes in the disk. Our belief is based on the fact that the amplitude of intensity fluctuations observed in QPOs is often quite large. Observations also show that QPOs have a finite frequency width, which indicates that the unstable modes in the disk have a finite life time (hence the term quasi-periodic oscillations). Apart from the rotation period, there are two

natural time scales in the disk: the time scale associated with the effective gravity, which is $\sim 1/\Omega_{\rm eff}$, and the viscous time scale, which is $\sim r/v_r$, where v_r is the mean radial velocity of the disk fluid. For a standard disk, $\Omega_{\rm eff} \sim c_s/r$, where c_s is the sound speed. Since $c_s \gg v_r$, the time scale $1/\Omega_{\rm eff}$ is generally much shorter than r/v_r. Therefore, the likely lifetime of blobs created by the instability is $1/\Omega_{\rm eff}$. Once a mass blob is formed, it will drift toward the central object under the action of gravity, causing a displacement in the center frequency and a width to the QPO feature in the power spectrum. The width is likely to be $\Delta f \sim \Omega_{\rm eff}/2\pi \sim (h/r)(\Omega_m/2\pi)$, where h is the vertical thickness of the disk, and the displacement speed is approximately $df/dt \sim (\Omega_{\rm eff}/2\pi)f$.

Another issue concerns how the presence of a nonaxisymmetric mode translates to a time modulation of the observed flux. Two possibilities are likely. One is that the system is viewed in a nearly edge-on configuration so that the accreting star eclipses the far side of the disk. Then, as bright and faint segments of the disk are successively eclipsed the signal at the observer will be modulated. The other possibility, which also requires fairly high inclination, is that the motion of the gas is relativistic and the observed signal is dominated by the blue-shifted segment of the disk. Once again, as the nonaxisymmetric pattern rotates, the signal will oscillate. Both mechanisms require that the bright and faint patches on the disk should have large areas, since otherwise the fractional modulation of the observed X-ray flux will be small.

The azimuthal extent of a bright patch in a nonaxisymmetric mode with wavenumber m is $\sim \pi/m$. The radial extent also has an m-dependence, since away from the magnetospheric radius the perturbation solutions decay with radius as $\sim r^{\pm m}$ (§4.1). For both reasons, low-m modes have patches with the largest area and hence are most promising. The area occupied by a bright patch, defined to correspond to an annular region in the disk bounded by a radius where the perturbation amplitude is half the peak, is estimated to be $S \sim (\pi r_m^2/2m)(4^{1/m} - 4^{-1/m})$. For $m = 1, 2, 3$ we have $S \sim 1.875\pi r_m^2, 0.375\pi r_m^2, 0.16\pi r_m^2$, respectively. For large m, S approaches zero according to $S \sim 2\pi r_m^2(\ln 2/m^2)$. The scaling clearly shows that low-m modes dominate by a large factor. In addition, as we argued earlier, low-m modes are likely to saturate with substantially larger amplitudes than high-m modes. This is yet another reason why only the lowest order few modes are expected to cause a discernible signal in the observations.

Apart from demonstrating that unstable modes exist and that mode frequencies in the ratio 2:3 are possible, the model does not really explain any of the many puzzling features seen in the observations (see the summary in §1). For instance, the model does not explain why the frequency difference between twin kHz QPOs in neutron star systems is often roughly of order the neutron star spin frequency (van der Klis 2000) or sometimes half the spin

frequency (Wijnands et al. 2003). Even though the version of the model described in §5 appears to have the necessary ingredients for the beat frequency model to operate, namely gas orbiting at Keplerian frequency around a magnetosphere that rotates at the stellar frequency, nevertheless our analysis does not reveal any beat phenomenon. Clearly, additional physics is needed beyond what we have considered here.

A Rayleigh-Taylor-like process has been studied extensively by Titarchuk and collaborators in a sub-Keplerian transition region of a disk around a black hole or a weakly magnetized neutron star (Titarchuk, Lapidus, & Muslimov 1998; Osherovich & Titarchuk 1999; Titarchuk, Osherovich,& Kuznetsov 1999; Titarchuk 2002, 2003). These authors focus only on stable modes and suggest that their model can explain the observed correlation between the twin kilohertz frequencies and the horizontal branch QPO frequency (Osherovich & Titarchuk 1999; Titarchuk 2003). In their model, the dynamical effect of the magnetic field is always assumed to be unimportant, so the fluid is described purely within hydrodynamics. The model assumes the existence of a thin sub-Keplerian transition region in the vicinity of the compact central object where the accreting matter adjusts itself either to the surface of a rotating neutron star or to the innermost boundary of the accretion disk (Titarchuk, Lapidus, & Muslimov 1998). But the origin of the transition layer is not explained, especially considering that the magnetic field is assumed to be weak.

The model described in the present paper (see §2.1) differs from Titarchuk's model in two respects. First, we assume that the magnetic field is dynamically important inside the inner edge of the disk. Second, we focus on genuinely unstable modes rather than on stable modes, since we assume that only unstable modes can grow to a large enough amplitude to produce the observed intensity fluctuations. Because of the assumption of a strong magnetic field, a narrow transition region develops naturally at the disk-magnetosphere interface of the model, and unstable oscillations are triggered at this interface.

Kaisig et al. (1992) used two-dimensional shearing box simulations to study the magnetic interchange instability in an accretion disk with a vertical magnetic field. When the magnetic field is strong and its strength decreases with increasing radius, they find that an instability develops spontaneously. The model we consider is an extreme version of the Kaisig et al. model in which the magnetic field decreases discontinuously at the magnetospheric radius. Our analytical results are consistent with Kaisig et al. (1992)'s numerical result that, in the linear regime, the growth rate of perturbations depends on the azimuthal wave number $k = m/r$ of the initial perturbations as $\omega_{\rm I} \sim k^{1/2}$. In both studies, the dependence of quantities on z is neglected. When this dependence is included, Lovelace, Romanova, & Newman (1994) showed that the twisting of field lines acts to drive winds or jets from the disk surfaces, which increases the disk accretion speed and so amplifies the magnetic field and

leads to runaway or implosive accretion and explosive wind or jet formation. Similar results have also been obtained by Lubow, Papaloizou & Pringle (1994a,b). [However, Lubow et al. 1994b also claimed the existence of stable solutions with no accretion and no wind.]

Lubow & Spruit (1995) and Spruit et al. (1995) found that disk shear tends to stabilize the disk-magnetosphere interface. This seems to be in conflict with our result that the growth rate of the Rayleigh-Taylor instability increases with increasing q. However, we stress that in their model the magnetic field has both vertical and radial components. Indeed, they modeled the disk as a sheet of zero thickness, so that the radial component of the magnetic field has a jump as one goes from below to above the disk. The pressure of gas and magnetic fields is negligible in the disk, but the magnetic curvature force appears in the equation of motion. This is very different from our model, where the disk has a nonzero (indeed infinite) thickness, the magnetic field has only a vertical component, the curvature force of the magnetic field is zero, and the magnetic pressure and gas pressure both play a dynamical role. Our model is perhaps more suitable for describing the central layer of the disk, while their model may be more applicable to the surface layers.

Chandran (2001) has considered the Rayleigh-Taylor instability of a strong vertical magnetic field confined by a disk threaded with a horizontal magnetic field. The aim of his study was to understand the equilibrium of magnetic flux tubes observed in the central regions of the Galaxy. Although the model has some points of similarity with the present study, there are also large differences. The disk in Chandran's model is assumed to have a uniform rotation and the gravitational potential is assumed to correspond to a constant background mass density (so that the gravitational acceleration increases linearly with radius). In contrast, we assume that the disk is differentially rotating and that the gravitational potential corresponds to that of a compact mass at the center. However, Chandran considers a compressible gas whereas we simplify our problem by taking the gas to be incompressible.

Chandran (2001) has derived a formula (his eqs. [91] and [92]) for the oscillation frequency when there is no magnetic field and the density contrast parameter $\mu = \pm 1$. His results are consistent with our analytical results for a disk with constant angular velocity (see our eq. [36]). In particular, the results confirm that the disk vorticity has the effect of stabilizing the modes.

The authors thank the anonymous referee for several useful comments. LXL's research was supported by NASA through Chandra Postdoctoral Fellowship grant number PF1-20018 awarded by the Chandra X-ray Center, which is operated by the Smithsonian Astrophysical Observatory for NASA under contract NAS8-39073. RN was supported in part by NASA grant NAG5-10780 and NSF grant AST 0307433.

A. A Necessary Condition for Disk Instability

A necessary condition for instability can be derived from the wave equation (19), following the approach pioneered by Howard (1961) (see also Li et al. 2003, Appendix B).

Defining $W = \varphi\sqrt{\sigma}$, equation (19) can be recast as

$$\frac{d}{dr}\left(r\rho_0\sigma\frac{d\varphi}{dr}\right) + \frac{m^2}{r^2}\left\{-\left[\frac{d\ln\rho_0}{d\ln r}\,\Omega_{\rm eff}^2 + \frac{1}{4}\left(r\frac{d\Omega}{dr}\right)^2\right]\frac{1}{\sigma} \right.$$
$$\left. -\sigma + \frac{2\zeta}{m}\frac{d\ln\left(\rho_0\Omega_\kappa\right)}{d\ln r} - \frac{r}{2m\rho_0}\frac{d}{dr}\left(r\rho_0\frac{d\Omega}{dr}\right)\right\} r\rho_0\varphi \;=\; 0\,. \tag{A1}$$

Multiplying equation (A1) by the complex conjugate variable φ^* and integrating over the whole flow yields

$$\int_{r_1}^{r_2}\left(\sigma\left|\frac{d\varphi}{dr}\right|^2 + \frac{m^2}{r^2}\left\{\left[\frac{d\ln\rho_0}{d\ln r}\,\Omega_{\rm eff}^2 + \frac{1}{4}\left(r\frac{d\Omega}{dr}\right)^2\right]\frac{1}{\sigma} + \sigma \right.\right.$$
$$\left.\left. -\frac{2\zeta}{m}\frac{d\ln\left(\rho_0\zeta\right)}{d\ln r} + \frac{r}{2m\rho_0}\frac{d}{dr}\left(r\rho_0\frac{d\Omega}{dr}\right)\right\}|\varphi|^2\right) r\rho_0 dr \;=\; r\rho_0\sigma\varphi^*\frac{d\varphi}{dr}\bigg|_{r_1}^{r_2}\,. \tag{A2}$$

Taking the boundary condition to be $W = 0$ at r_1 and r_2, we see that the right-hand side of equation (A2) vanishes. Then, the imaginary part of the left-hand side of equation (A2) must vanish[3]

$$\omega_{\rm I}\int_{r_1}^{r_2}\left(\left|\frac{d\varphi}{dr}\right|^2 + \frac{m^2}{r^2}\left\{-\left[\frac{d\ln\rho_0}{d\ln r}\,\Omega_{\rm eff}^2 + \frac{1}{4}\left(r\frac{d\Omega}{dr}\right)^2\right]\frac{1}{|\sigma|^2} + 1\right\}|\varphi|^2\right) r\rho_0 dr = 0\,, \tag{A3}$$

where $\omega_{\rm I} \equiv \Im(\omega) = \Im(\sigma)$. The integral in equation (A3) is positive, and therefore $\omega_{\rm I} = 0$, unless the condition,

$$R_{\rm eff} < \frac{1}{4}\,, \tag{A4}$$

is satisfied somewhere in the region of integration, where

$$R_{\rm eff} \equiv -\frac{d\ln\rho_0}{d\ln r}\left(r\frac{d\Omega}{dr}\right)^{-2}\Omega_{\rm eff}^2 = -\left(\frac{\Omega_{\rm eff}}{\Omega}\right)^2\left(\frac{d\ln\Omega}{d\ln r}\right)^{-2}\frac{d\ln\rho_0}{d\ln r}\,. \tag{A5}$$

Note that $\Omega_{\rm eff}^2$ can be either positive or negative.

Therefore, a necessary condition for the existence of instability (i.e., $\omega_{\rm I} \neq 0$) is that the inequality (A4) must hold somewhere in the disk. Obviously, the converse of the inequality, i.e. $R_{\rm eff} \geq 1/4$, is a sufficient condition for stability.

---

[3]If the boundary condition is taken to be $dW/dr = 0$, then it can be shown that the right-hand side of eq. (A2) is real, and the result is still the same.

B. Classical Rayleigh-Taylor and Kelvin-Helmholtz Instability

Let us start from the hydrodynamic equations (1) and (2) (with $\mathbf{B} = 0$), and use Cartesian coordinates (x, y, z). If the fluid is incompressible, equation (1) becomes equations (5) and (6). Let us assume that the system is two-dimensional and that all quantities are independent of z. We take gravity to be in the x direction: $\mathbf{g} = -\nabla\Phi(x) = -g(x)\mathbf{e}_x$. For the unperturbed equilibrium state we assume that $\rho = \rho_0(x)$, $p = p_0(x)$, and $\mathbf{v} = V(x)\mathbf{e}_y$. Then, the equilibrium in the x-direction is given by

$$g = -\frac{1}{\rho_0}\frac{dp_0}{dx} \ . \tag{B1}$$

Consider now linear perturbations

$$\left\{ \begin{array}{c} \delta\rho \\ \delta p \\ \delta\mathbf{v} \end{array} \right\} = \left\{ \begin{array}{c} \rho_1(x) \\ p_1(x) \\ u(x)\,\mathbf{e}_x + v(x)\,\mathbf{e}_y \end{array} \right\} \times e^{-i\omega t + ik_y y} \ , \tag{B2}$$

where ω and k_y are constants. The first order perturbations of equations (5) and (6) then give

$$\frac{du}{dx} + ik_y v = 0 \ , \tag{B3}$$

$$i\sigma - u\frac{d\rho_0}{dx} = 0 \ , \tag{B4}$$

respectively, where

$$\sigma \equiv \omega - k_y V \ . \tag{B5}$$

The first order perturbation of equation (13), which is derived from equation (5) and the curl of equation (2), leads to

$$\frac{1}{\rho_0}\frac{d}{dx}\left(\rho_0 v\right) + \left[\frac{i}{\sigma\rho_0}\frac{d}{dx}\left(\rho_0\frac{dV}{dx}\right) - ik_y\right] u = -\frac{\rho_1}{\rho_0}\frac{k_y}{\sigma}g \ . \tag{B6}$$

¿From equations (B3)–(B6) we can derive a wave equation for u,

$$\frac{1}{\rho_0}\frac{d}{dx}\left(\rho_0\frac{du}{dx}\right) - k_y^2\left[\frac{g}{\sigma^2 x}\frac{d\ln\rho_0}{d\ln x} - \frac{2\zeta}{k_y x\sigma}\frac{d\ln\left(\rho_0\zeta\right)}{d\ln x} + 1\right] u = 0 \ , \tag{B7}$$

where the vorticity ζ is given by

$$\zeta \equiv \frac{1}{2}\frac{dV}{dx} \ . \tag{B8}$$

As in the main paper, we can derive the following two junction conditions at a surface of discontinuity at $x = 0$:

$$\Delta_m \left(\frac{u}{\sigma} \right) = 0 \ , \tag{B9}$$

$$\Delta_m \left[\sigma \rho_0 \frac{du}{dx} - k_y \left(\frac{k_y g}{\sigma} - 2\zeta \right) \rho_0 u \right] = 0 \ . \tag{B10}$$

where $\Delta_m(f) \equiv f(x = 0^+) - f(x = 0^-)$.

Following Drazin & Reid (1981, Chapter 4, except that we switch x and z to be consistent with the convention in this paper), we assume for the unperturbed equilibrium state

$$\rho = \begin{cases} \rho_- \ , & \text{if } x < 0 \\ \rho_+ \ , & \text{if } x > 0 \end{cases} \ , \qquad \mathbf{v} = \begin{cases} V_- \, \mathbf{e}_y \ , & \text{if } x < 0 \\ V_+ \, \mathbf{e}_y \ , & \text{if } x > 0 \end{cases} \ , \tag{B11}$$

where ρ_-, ρ_+, V_-, and V_+ are constants. Then, on each side of $x = 0$, we have $\zeta = 0$ and $d\rho/dx = 0$, and the solutions of the wave equation (B7) are $u \propto \exp(\pm k_y x)$. Requiring that $u(x \to \pm\infty) = 0$, then from the junction conditions (B9) and (B10) we can solve for the eigenvalue for the frequency (assuming that $k_y > 0$) to obtain

$$\omega = k_y \frac{\rho_+ V_+ + \rho_- V_-}{\rho_+ + \rho_-} \pm \sqrt{ - \frac{\rho_+ - \rho_-}{\rho_+ + \rho_-} \, k_y g - \frac{\rho_+ \rho_-}{\rho_+ + \rho_-} \, k_y^2 \left(V_+ - V_- \right)^2 } \ . \tag{B12}$$

Equation (B12) is exactly the same as equation (4.20) in Drazin & Reid (1981), provided we substitute their s with our $-i\omega$, and their subscripts "1" and "2" with our subscripts "$-$" and "$+$", respectively. The first term under the square root in equation (B12) represents the Rayleigh-Taylor instability, while the second term represents the Kelvin-Helmholtz instability.

The analysis presented in the main paper goes beyond this classical analysis in a few respects. We include rotation (and correspondingly vorticity), our flow has shear (actually differential rotation), and we consider a density gradient. These additional features modify some of the results, but the basic physics remains the same, namely the presence of the Rayleigh-Taylor and Kelvin-Helmholtz instabilities.

REFERENCES

Abramowicz, M. A., & Kluzniak, W. 2001, A&A, 374, L19

Abramowicz, M. A., Bulik, T., Bursa, M., & Kluzniak, W 2003, A&A, 404, L21

Alpar, M. A., & Shaham, J. 1985, Nature, 316, 239

Arons, J., & Lea, S. M. 1976a, ApJ, 207, 914

Arons, J., & Lea, S. M. 1976b, ApJ, 210, 792

Balbus, S. A., & Hawley, J. F. 1998, Rev. Mod. Phys., 70, 1

Belloni, T., Psaltis, D., & van der Klis, M. 2002, ApJ, 572, 392

Bisnovatyi-Kogan, G. S., & Ruzmaikin, A. A. 1974, Ap&SS, 28, 45

Bisnovatyi-Kogan, G. S., & Ruzmaikin, A. A. 1976, Ap&SS, 42, 401

Bradt, H. V., Rothschild, R. E., & Swank, J. H 1993, A&AS, 97, 355

Chandran, B. D. G. 2001, ApJ, 562, 737

Chandrasekhar, S. 1961, Hydrodynamic and Hydromagnetic Stability (Oxford: Clarendon Press)

Di Salvo, T., Méndez, M., & van der Klis, M. 2003, A&A, 406, 177

Drazin, P. G., & Reid, W. H. 1981, Hydrodynamic Stability (Cambridge: Cambridge University Press)

Elsner, R., & Lamb, F. K. 1976, Nature, 262, 356

Elsner, R., & Lamb, F. K. 1977, ApJ, 215, 897

Elsner, R., & Lamb, F. K. 1984, ApJ, 278, 326

Ghosh, P., & Lamb, F. K. 1978, ApJ, 223, L83

Ghosh, P., & Lamb, F. K. 1979, ApJ, 232, 259

Goldreich, P., Goodman, J., & Narayan, R. 1986, MNRAS, 221, 339

Howard, L. N. 1961, J. Fluid Mech., 10, 509

Igumenshchev, I. V., Narayan, R., & Abramowicz, M. A. 2003, ApJ, 592, 1042

Ikhsanov, N. R., & Pustil'nik, L. A. 1996, A&A, 312, 338

Kaisig, M., Tajima, T., & Lovelace, R. V. E. 1992, ApJ, 386, 83

Kato, S. 2001a, PASJ, 53, 1

Kato, S. 2001b, PASJ, 53, L37

Kato, S. 2002, PASJ, 54, 39

Kato, S. 2003, PASJ, 55, 257

Kato, S., Fukue, J., & Mineshige, S. 1998, Black-Hole Accretion Disks (Kyoto: Kyoto University Press)

Lamb, F. K., & Miller, M. C. 2001, ApJ, 554, 1210

Lamb, F. K., & Miller, M. C. 2003, ApJ Letters, submitted (astro-ph/0308179)

Lamb, F. K., Shibazaki, N., Alpar, M. A., & Shaham, J. 1985, Nature, 317, 681

Lewin, W. H. G., van Paradijs, J., & van der Klis, M. 1988, Space Sci. Rev., 46, 273

Li, L. -X., Goodman, J., & Narayan, R. 2003, ApJ, 593, 980

Livio, M., Pringle, J. E., & King, A. R. 2003, ApJ, in press (astro-ph/0304367)

Lovelace, R. V. E., Romanova, M. M., & Newman, W. I. 1994, ApJ, 437, 136

Lubow, S. H., & Spruit, H. C. 1995, ApJ, 445, 337

Lubow, S. H., Papaloizou, J. C. B., & Pringle, J. E. 1994a, MNRAS, 267, 235

Lubow, S. H., Papaloizou, J. C. B., & Pringle, J. E. 1994b, MNRAS, 268, 1010

Michel, F. C. 1977a, ApJ, 213, 836

Michel, F. C. 1977b, ApJ, 214, 261

Migliari, S., van der Klis, M., & Fender, R. 2003, MNRAS, in press (astro-ph/0309288)

Miller, M. C., Lamb, F. K., & Psaltis, D. 1998, ApJ, 508, 791

Narayan, R., Goldreich, P., & Goodman, J. 1987, MNRAS, 228, 1

Narayan, R., Igumenshchev, I. V., & Abramowicz, M. A. 2003, PASJ, submitted (astro-ph/0305029)

Nowak, M. A., & Wagoner, R. V. 1991, ApJ, 378, 656

Nowak, M. A., & Wagoner, R. V. 1992, ApJ, 393, 697

Nowak, M. A., Wagoner, R. V., Begelman, M. C., & Lehr, D. E. 1997, ApJ, 477, L91

Okazaki, A. T., Kato, S., & Fukue, J. 1987, PASJ, 39, 457

Ortega-Rodriguez, M., & Wagoner, R. V. 2000, ApJ, 537, 922

Osherovich, V., & Titarchuk, L. 1999, ApJ, 522, L113

Papaloizou, J. C. B., & Pringle, J. E. 1985, MNRAS, 213, 799

Perez, C. A., Silbergleit, A. S., Wagoner, R. V., & Lehr, D. E. 1997, ApJ, 476, 589

Psaltis, D., Belloni, T., & van der Klis, M. 1999, ApJ, 520, 262

Remillard, R. A., Muno, M. P., McClintock, J. E., & Orosz, J. A. 2002a, ApJ, 580, 1030

Remillard, R. A., Muno, M. P., McClintock, J. E., & Orosz, J. A. 2002b, Proceedings. of the 4th Microquasar Workshop, 2002, ed. Ph. Durouchoux, Y. Fuchs, & J. Rodriguez (Center for Physics: Kolkata); astro-ph/0208402

Silbergleit, A., Wagoner, R. V., & Ortega-Rodríguez, M. 2001, ApJ, 548, 335

Spruit, H. C., & Taam, R. E. 1990, A&A, 229, 475

Spruit, H. C., Stehle, R., & Papaloizou, J. C. B. 1995, MNRAS, 275, 1223

Stella, L., & Vietri, M. 1998, ApJ, 492, L59

Stella, L., & Vietri, M. 1999, Phys. Rev. Lett., 82, 17

Stella, L., Vietri, M., & Morsink, S. M. 1999, ApJ, 524, L63

Strohmayer, T. E., Zhang, W., Swank, J. H., Smale, A., Titarchuk, L., Day, C., & Lee, U. 1996, ApJ, 469, L9

Titarchuk, L. 2002, ApJ, 578, L71

Titarchuk, L. 2003, ApJ, 591, 354

Titarchuk, L., Lapidus, I., & Muslimov, A. 1998, ApJ, 499, 315

Titarchuk, L., Osherovich, V., & Kuznetsov, S. 1999, ApJ, 525, L129

van der Klis, M. 1997, Astronomical Time Series, ed. D. Maoz, A. Sternberg, & E.M. Leibowitz (Dordrecht: Kluwer), p. 121

van der Klis, M. 1998, The Many Faces of Neutron Stars. ed. R. Buccheri, J. van Paradijs, & M. A. Alpar (Dordrecht: Kluwer), p. 337

van der Klis, M. 2000, ARA&A, 38, 717

Wagoner, R. V. 1999, Phys. Rep., 311, 259

Wagoner, R. V., Silbergleit, A. S., & Ortega-Rodriguez, M. 2001, ApJ, 559, L25

Warner, B., Woudt, P. A., & Pretorius, M. L. 2003, MNRAS, in press (astro-ph/0306085)

Wijnands, R., van der Klis, M., Homan, J., Chakrabarty, D., Markwardt, C. B., & Morgan, E. H. 2003, Nature, 424, 44

Zhang, W., Strohmayer, T. E., & Swank, J. H. 1997, ApJ, 482, L167

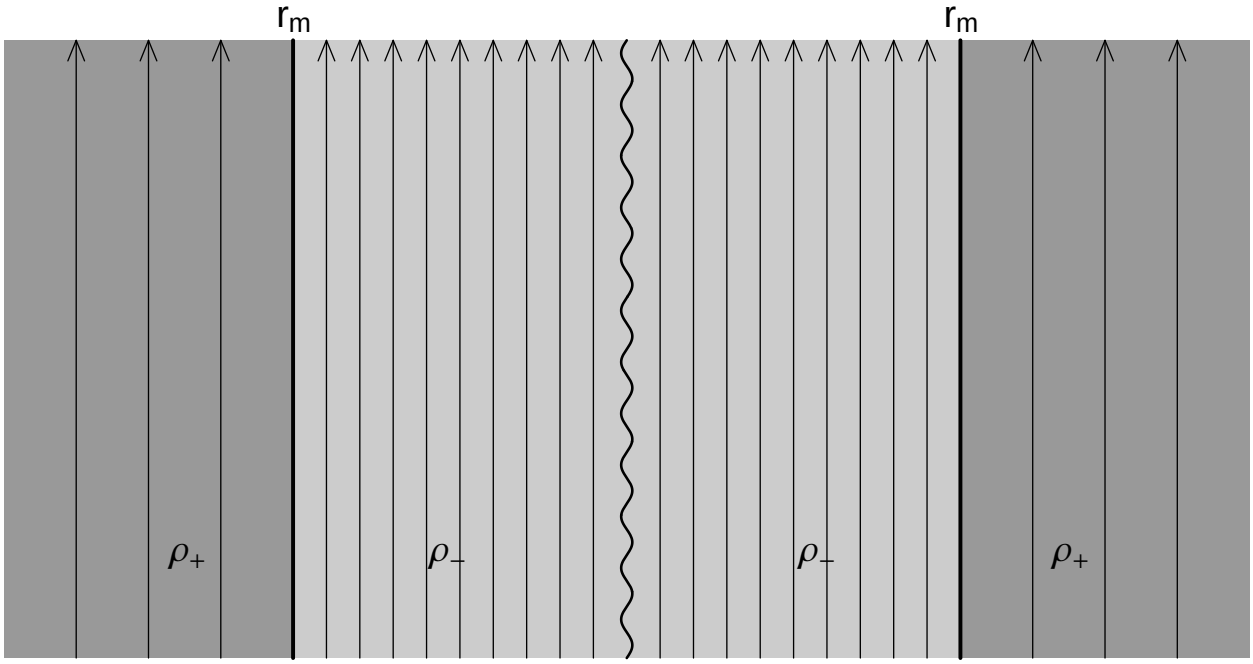

Fig. 1.— Schematic representation of the (r, z)-section of the cylindrical disk model studied in the paper. The wavy line represents the central compact star. The two thick vertical lines represent the radius $r = r_m$ which separates the magnetosphere on the inside from the accretion disk on the outside. The thin vertical lines with arrows show magnetic field lines. In the region $r > r_m$, the mass density (ρ_+) is high but the magnetic field is weak. In the region $r < r_m$, the mass density (ρ_-) is low but the magnetic field is strong. The jump in the mass density at $r = r_m$ is described by the parameter μ defined in eq. (29).

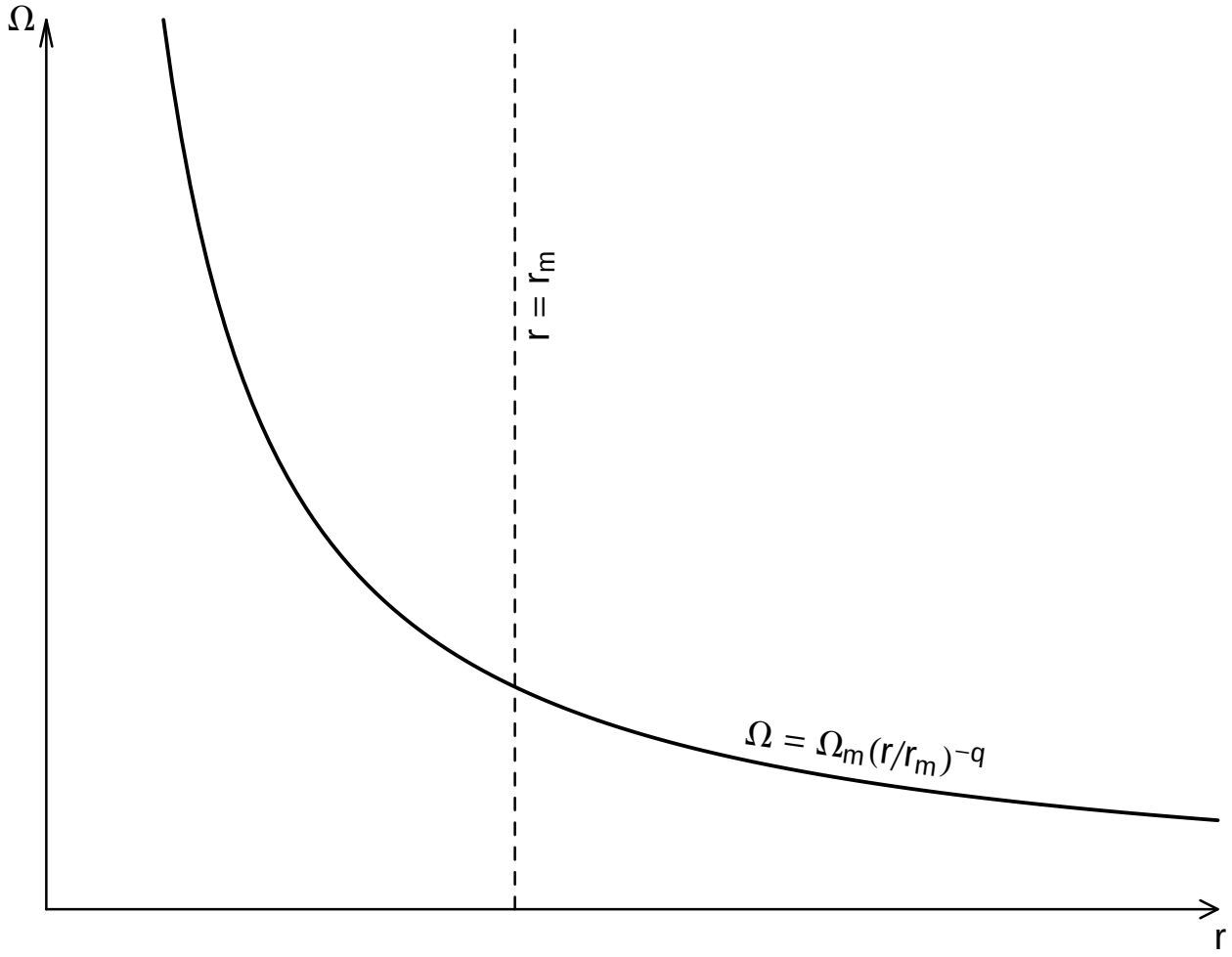

Fig. 2.— Disk angular velocity as a function of radius for the case of a central black hole (§4.1). The vertical dashed line marks the magnetospheric radius r_m. The angular velocity is taken to be continuous across this boundary.

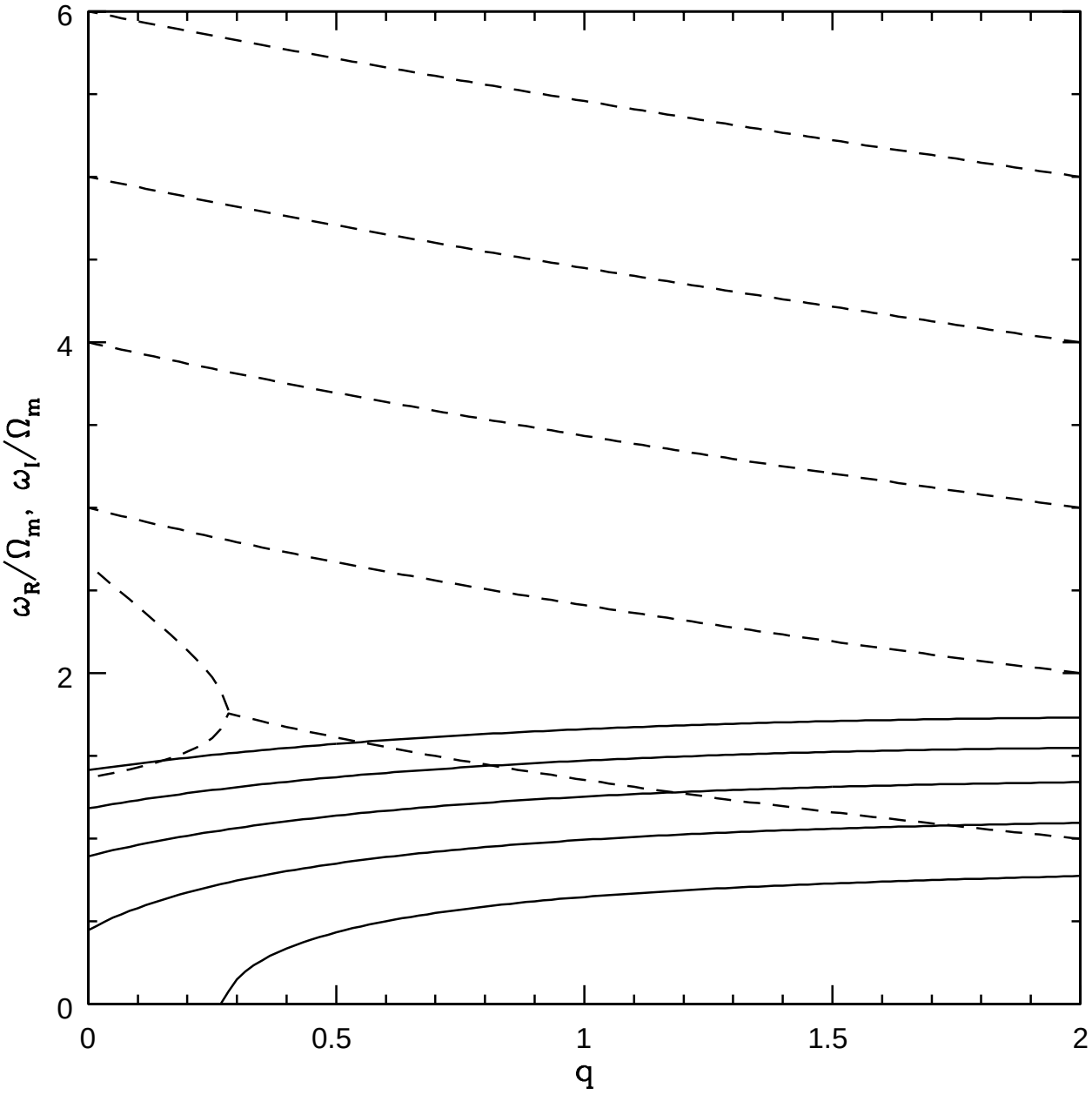

Fig. 3.— Numerical solutions for the mode frequency as a function of q (defined by $\Omega \propto r^{-q}$). The mass density has a jump at $r = r_m$ corresponding to $\mu = 1$, and the density is assumed to be constant on the two sides of the boundary. The effective gravity is given by $\Omega^2_{\mathrm{eff},m} = 0.6\Omega^2_m$. Solid lines correspond to the imaginary part of the frequency and measure the growth rates of the modes. Dashed lines correspond to the real part of the frequency and represent the observed oscillation frequencies. The different lines correspond to m = 1, 2, 3, 4, and 5 (bottom to top).

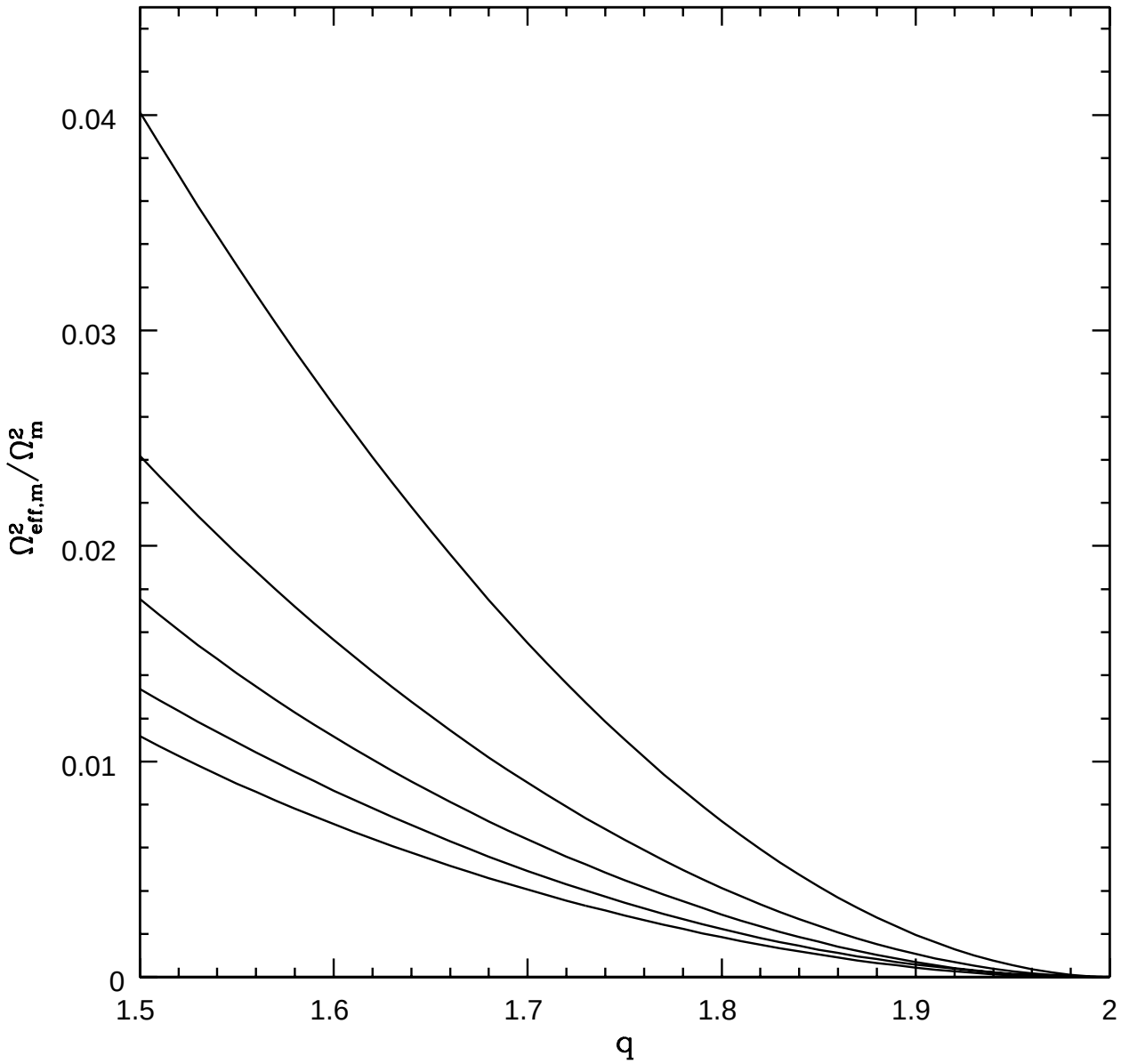

Fig. 4.— Critical effective gravity frequency $\Omega^2_{{\rm eff},m}$, which separates stable and unstable modes, for $3/2 \leq q \leq 2$. It is assumed that $\mu = 1$ and $\gamma = 0$. The different lines correspond to $m = 1$, 2, 3, 4, and 5 (top to bottom). Each line separates the q-$\Omega^2_{{\rm eff},m}$ plane into two regions: above the line modes of the given m are unstable, and below the line the modes are stable.

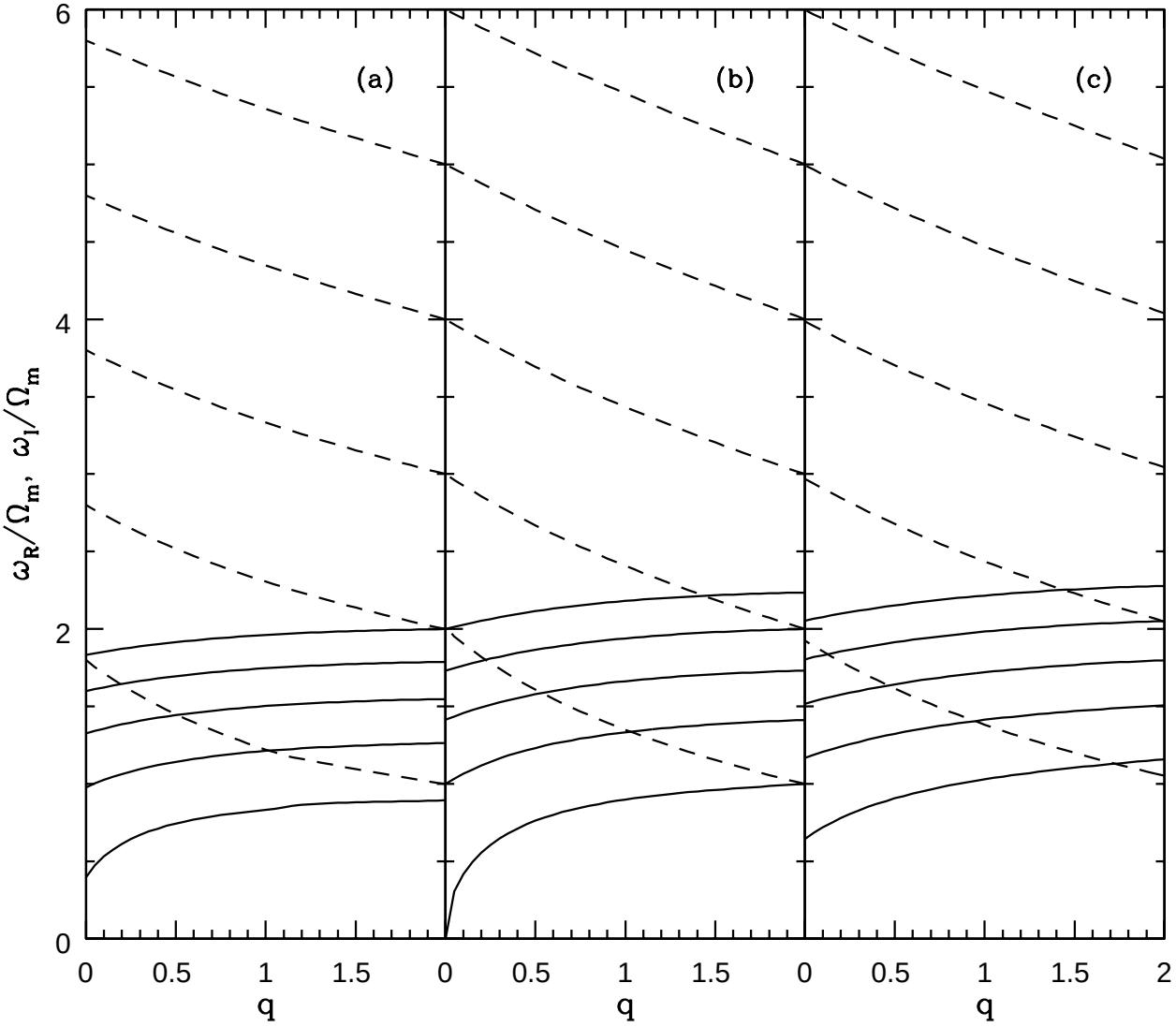

Fig. 5.— Similar to Fig. 3, but (a) $\mu = 0.8$, $\Omega^2_{\mathrm{eff},m} = \Omega^2_m$, and the mass density is constant on both sides of $r = r_\mathrm{s}$; (b) $\mu = 1$, $\Omega^2_{\mathrm{eff},m} = \Omega^2_m$, and the mass density is constant on both sides of $r = r_m$; (c) $\mu = 1$, $\Omega^2_{\mathrm{eff},m} = \Omega^2_m$, and the mass density is constant for $r < r_m$, but decays with increasing radius according to $\rho \propto r^{-1}$ for $r > r_m$.

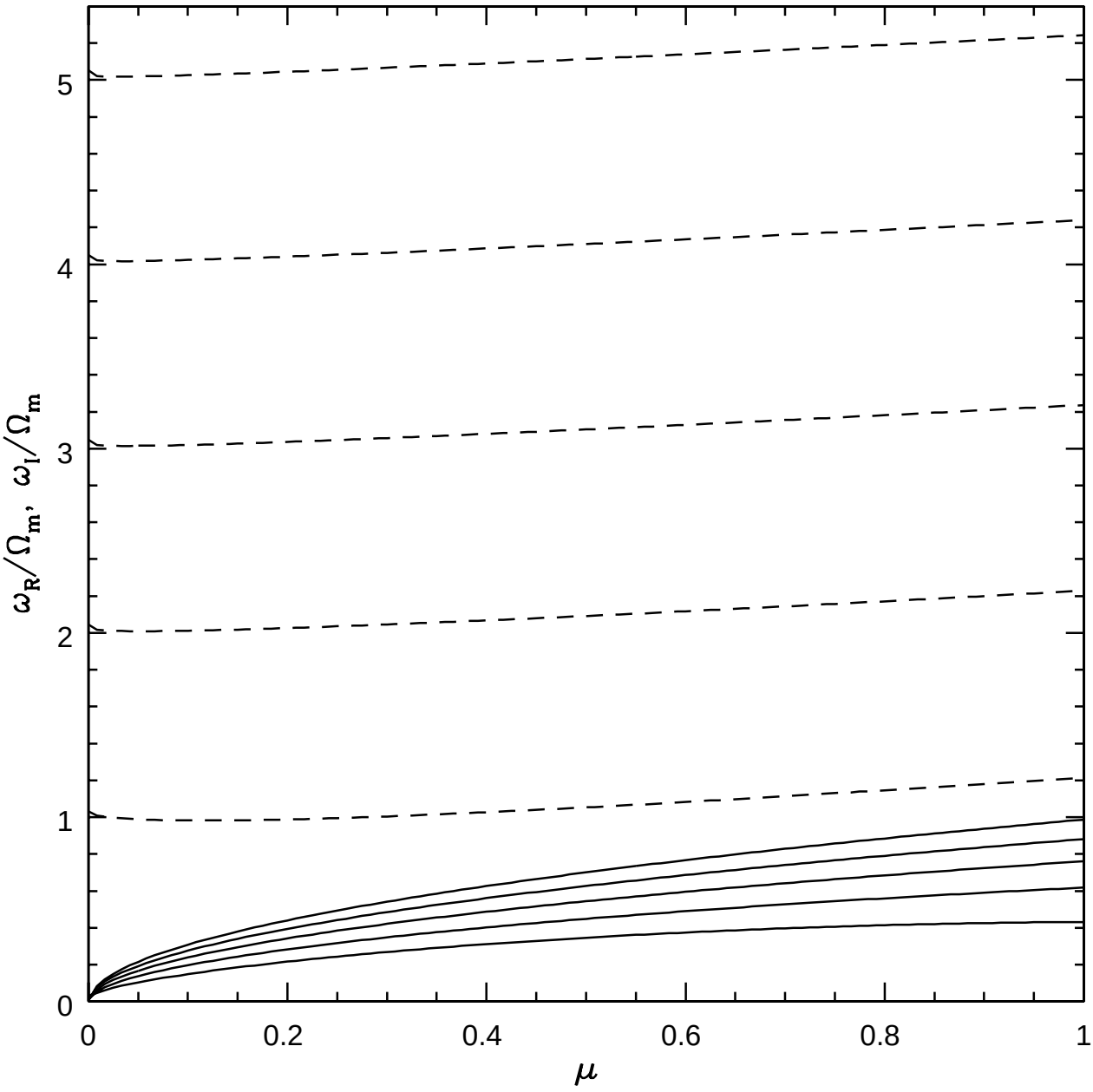

Fig. 6.— Mode frequencies as a function of μ (defined by the jump in mass density at $r = r_m$) for a Keplerian-type disk ($q = 3/2$). The mass density is constant for $r < r_{\rm m}$, but decays with increasing radius according to $\rho \propto r^{-1}$ for $r > r_m$. At $r = r_m$ the effective gravity frequency is $\Omega^2_{{\rm eff},m} = 0.2\Omega^2_m$. Solid lines correspond to the imaginary part of the frequency and dashed lines to the real part of the frequency. The different lines correspond to $m = 1$, 2, 3, 4, and 5 (bottom to top).

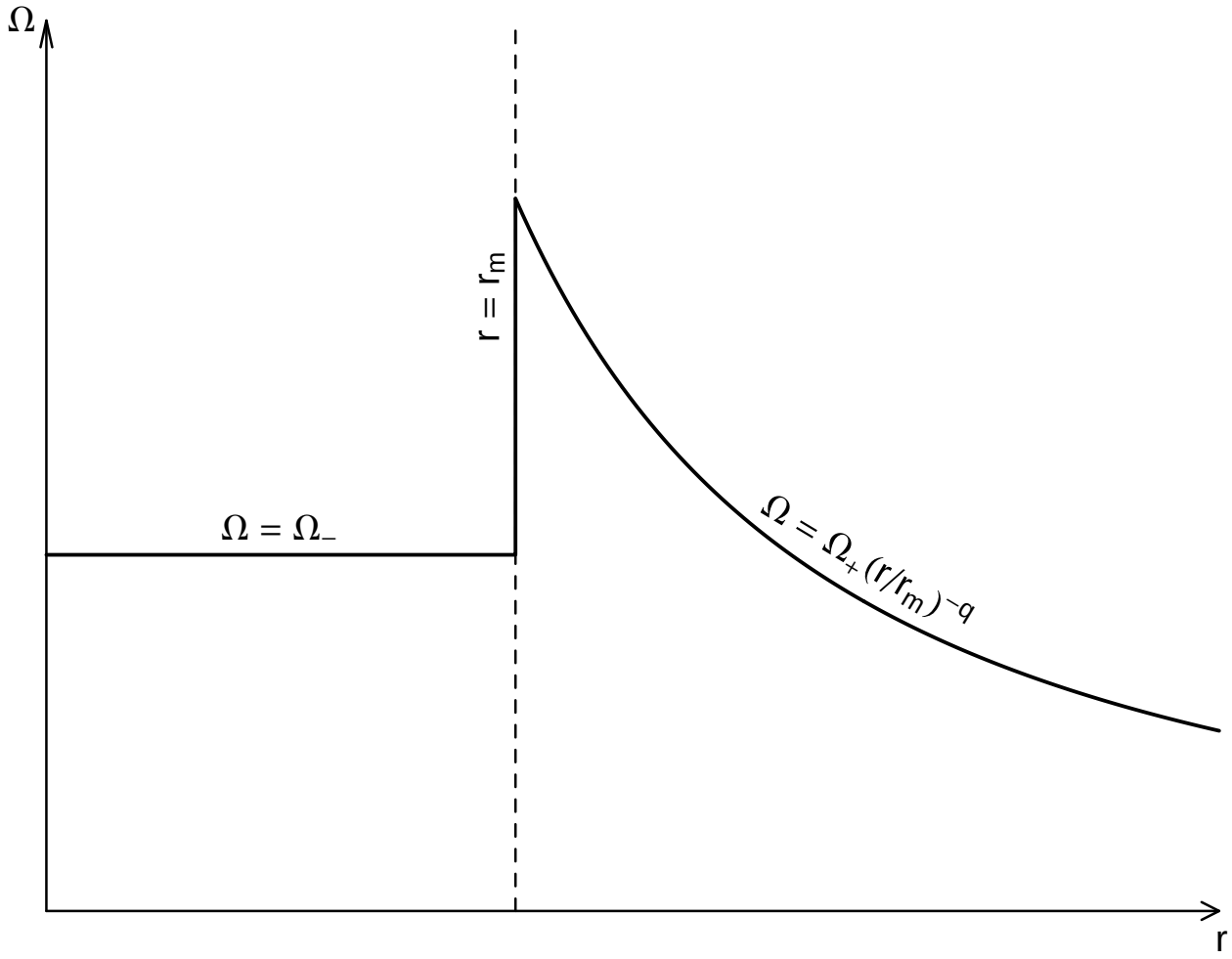

Fig. 7.— Disk angular velocity as a function of radius for the case of a magnetized neutron star (§4.2). The vertical dashed line marks the magnetospheric radius r_m. The angular velocity has a jump at r_m: $\Delta_m(\Omega) = \Omega_+ - \Omega_- \neq 0$. The jump may be either positive or negative.

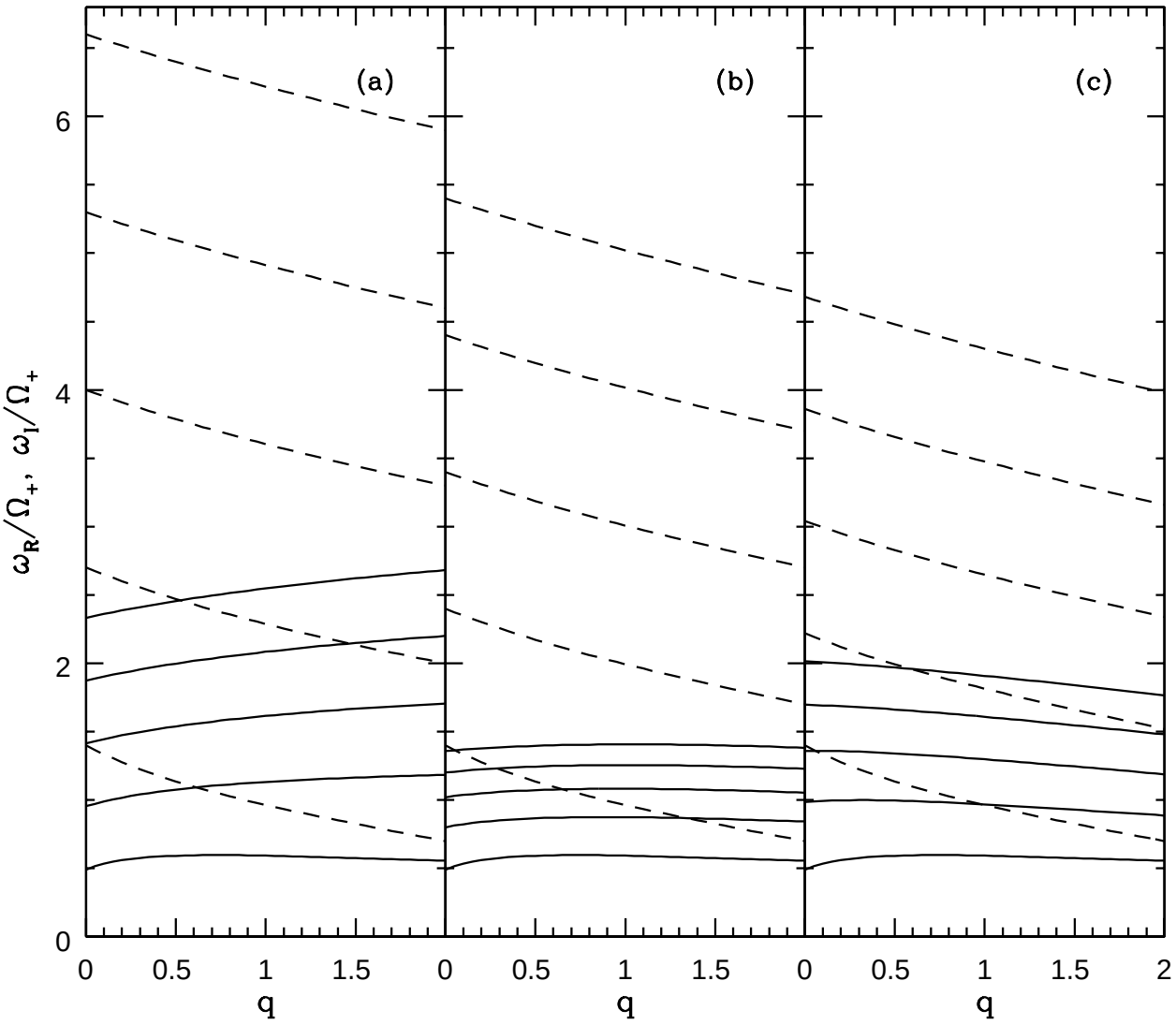

Fig. 8.— Mode frequencies for a disk with an angular frequency jump at r_m: $\Omega = \Omega_- =$ constant for $r < r_m$, and $\Omega = \Omega_+(r/r_m)^{-q}$ for $r > r_m$. The mass density is constant away from $r = r_m$, but has a jump at r_m with $\mu = 0.4$. At $r = r_{m+}$, it is assumed that $\Omega^2_{\rm eff,+} = \Omega^2_+$. (a) The angular velocity is assumed to satisfy $\Omega_- = 2\Omega_+$. (b) $\Omega_- = \Omega_+$. (c) $\Omega_- = 0.4\Omega_+$. Line types have the same meanings as in Fig. 3.